REPUBLIC OF TURKEY

AKDENIZ UNIVERSITY

BOWEL ACTIVITY DETECTION ALGORITHM WITH ACTIVE NOISE CANCELLATION FOR IOT DEVICES

Erdinç TÜRK

INSTITUTE OF NATURAL AND APPLIED SCIENCES

DEPARTMENT OF COMPUTER ENGINEERING

MASTER THESIS

JULY 2020

ANTALYA

REPUBLIC OF TURKEY

AKDENIZ UNIVERSITY

BOWEL ACTIVITY DETECTION ALGORITHM WITH ACTIVE NOISE CANCELLATION FOR IOT DEVICES

Erdinç TÜRK

INSTITUTE OF NATURAL AND APPLIED SCIENCES

DEPARTMENT OF COMPUTER ENGINEERING

MASTER THESIS

JULY 2020

ANTALYA

ÖZET

IOT CİHAZLARI İÇİN AKTİF GÜRÜLTÜ ÖNLEME ÖZELLİKLİ BAĞIRSAK SESİ TESPİT ALGORİTMASI

Erdinç TÜRK

Yüksek Lisans Tezi, Bilgisayar Mühendisliği Anabilim Dalı

Danışman: Doç. Dr. Ümit Deniz ULUŞAR

Temmuz 2020; 55 sayfa

Nesnelerin interneti sağlık hizmetlerinde çeşitli uygulamalara olanak sağlamaktadır. Buna örnek olarak kalp atışı, bağırsak aktivitesi, akciğer sesi gibi hastaların fizyolojik bilgilerini izlemek için kullanılan kablosuz tıbbi sensörler verilebilir. Karın bölgesinden ameliyat geçiren hastalarda bağırsak aktivitesinin gerçek zamanlı tespiti hastanın iyileşme süreci için büyük önem taşımaktadır. Çünkü, ameliyat sonrasında bağırsak hareketliliği geçici olarak durmaktadır. Bağırsak hareketliliği geri kazanılana kadar hasta aç bırakılmakta ve sonrasında hasta sıvı gıda ile beslenmektedir. Bağırsak hareketliliğini izlemek ve bağırsak aktivitesini otomatik olarak tespit etmek için birçok çalışma yapılmıştır. Ancak kliniklerde meydana gelen çevresel gürültüler nedeniyle aktivite tespiti zorlaşmaktadır.

Bu çalışmada, daha önceki çalışmalarımızda geliştirdiğimiz kablosuz elektronik stetoskop için aktif gürültü önleme özelliğine sahip bağırsak aktivitesi tespit algoritması geliştirildi. Çalışmanın odak noktası, elektronik stetoskopta bulunan iki mikrofonu kullanarak etkili bir aktif gürültü önleme uygulaması geliştirmektir. Deneyler hem sentetik hem de gerçek oskültasyon verileri kullanılarak geliştirildi. Aktif gürültü önleme için beş farklı adaptif filtre test edildi ve ideal bir adaptif filtre algoritması belirlendi. Sonrasında, bağırsak aktivitesi tespit algoritması gerçek oskültasyon verileri kullanılarak geliştirildi. Sinyal iyileştirme için aktif gürültü önleme uygulaması, bant geçiren filtre, sinyal normalizasyonu ve Hilbert dönüşümü teknikleri uygulandı. Oluşturulan ROC eğrisinden belirlenen genlik eşik değeri kullanılarak bağırsak sesleri tespit edildi. Algoritma, on farklı oskültasyon kaydı üzerinde test edildi ve bağırsak seslerinin tanınmasında %95,09 duyarlılık ve %95,83 özgüllük elde edildi.

ANAHTAR KELİMELER: Aktif Gürültü Önleme, Bağırsak Aktivitesi Tespiti, Elektronik Stetoskop, E-Sağlık, Nesnelerin İnterneti

JÜRİ: Doç. Dr. Ümit Deniz ULUŞAR

Prof. Dr. Atila YILMAZ

Dr. Öğr. Üyesi Taner DANIŞMAN

ABSTRACT

BOWEL ACTIVITY DETECTION ALGORITHM WITH ACTIVE NOISE CANCELLATION FOR IOT DEVICES

Erdinç TÜRK

MSc Thesis in Computer Engineering

Supervisor: Assoc. Prof. Dr. Ümit Deniz ULUŞAR

July 2020; 55 pages

Internet of Things (IoT) enables a variety of applications in healthcare. A key application for IoT based technologies is wireless medical sensors that can be used to monitor patients' physiological information such as heartbeat, bowel activity, lung sound. Real-time detection of bowel motility after major abdominal surgery has significant importance in the patients' healing process. Because intestinal motility temporarily stops after the surgery, a period of fasting is commonly practiced, and patients are fed with fluids following the recovery of bowel motility. Many studies have been conducted to monitor intestinal motility and automatically detect bowel activity. But bowel activity detection suffers from ambient noise occurs in clinics.

In this study, a bowel activity detection algorithm with active noise canceling feature was developed for our custom design IoT-driven electronic stethoscope, which was developed in our previous studies. This study's focus is to develop an effective active noise cancellation application by using both microphones of the electronic stethoscope. Experiments were conducted using both synthetic and real auscultation data. Five different adaptive filters were tested for active noise cancellation, and an ideal adaptive filter algorithm was determined. Then, a bowel activity detection algorithm was developed using real auscultation data. Active noise cancellation, bandpass filter, signal normalization, and Hilbert transform techniques were applied for signal enhancement. Bowel sounds were detected using an amplitude threshold value, which is determined from the generated ROC curve. The algorithm was tested on ten different auscultation recordings, and a sensitivity of 95.09% and a specificity of 95.83% were obtained in bowel sound recognition.

KEYWORDS: Active noise cancellation, Bowel activity detection, eHealth, Electronic stethoscope, Internet of things

COMMITTEE: Assoc. Prof. Dr. Ümit Deniz ULUŞAR

Prof. Dr. Atila YILMAZ

Asst. Prof. Dr. Taner DANIŞMAN

ACKNOWLEDGEMENTS

I would like to express my sincere appreciation to my advisor, Assoc. Prof. Dr. Ümit Deniz Uluşar, who helped, guided, and motivated me during this study. He integrated me into this field and steered me in the right direction with his invaluable knowledge and experience.

I would like to thank my colleagues at ComNets Laboratory for their assistance in device development and data collection during the study. I would also like to thank my colleagues at the department of computer engineering who have always been a great support.

Finally, I would like to express my very profound gratitude to my wife, Ezgi Özekinci Türk, for her endless patience, love, and support.

LIST OF CONTENTS

ÖZET i
ABSTRACT ii
ACKNOWLEDGEMENTS iii
TEXT OF OATH vi
SYMBOLS AND ABBREVIATIONS vii
LIST OF FIGURES viii
LIST OF TABLES xi
1. INTRODUCTION 1
2. LITERATURE REVIEW 3
 2.1. Bowel Sound Characteristics 3
 2.2. Adaptive Filters 4
  2.2.1. The least-mean-square (LMS) algorithm 7
  2.2.2. The normalized LMS (NLMS) algorithm 8
  2.2.3. Affine projection (AP) adaptive filter 9
  2.2.4. The recursive least-squares (RLS) algorithm 10
  2.2.5. Adaptive lattice (AL) filter 11
 2.3. Noise Modelling 12
 2.4. IoT-Driven Electronic Stethoscope 14
3. MATERIAL AND METHOD 18
 3.1. Adaptive Filter Algorithm Determination for Active Noise Cancellation 19
  3.1.1. Electronic stethoscope system identification 20
  3.1.2. Application of active noise cancellation 24
  3.1.3. ANC application on synthetic auscultation data 26
  3.1.4. ANC application on real auscultation data 29
 3.2. Bowel Activity Detection Algorithm 30
  3.2.1. Signal processing steps 30
  3.2.2. Detection of bowel activity 32
4. RESULTS AND DISCUSSION 35
 4.1. Results of Active Noise Cancellation Applications 35
  4.1.1. Results of ANC on synthetic auscultation data 35
  4.1.2. Results of ANC on real auscultation data 38

4.2. Results of Bowel Activity Detection 51
5. CONCLUSION 53
6. REFERENCES 54
RESUME

TEXT OF OATH

I declare that this study "Bowel Activity Detection Algorithm with Active Noise Cancellation for IoT Devices”, which I present as master thesis, is in accordance with the academic rules and ethical conduct. I also declare that I cited and referenced all material and results that are not original to this work.

17/07/2020

Erdinç TÜRK

SYMBOLS AND ABBREVIATIONS

Abbreviations

ADC	: Analog to Digital Converter
AL	: Adaptive Lattice
ANC	: Active Noise Cancellation
AP	: Affine Projection
AWGN	: Additive White Gaussian Noise
BA	: Bowel Activity
BN	: Background Noise
BS	: Bowel Sound
dB	: Decibel
FIR	: Finite Impulse Response
Hz	: Hertz
IN	: Impulsive Noise
IoT	: Internet of Things
LMS	: Least Mean Square
MB	: Multiple Burst
MSE	: Mean Square Error
NLMS	: Normalized Least Mean Square
QP	: Quiet Period
ROC	: Receiver Operating Characteristics
RLS	: Recursive Least Square
SB	: Single Burst
WGN	: White Gaussian Noise

LIST OF FIGURES

Figure 2.1. Auscultation samples under different cases (QP, Noise, SB, MB)................3
Figure 2.2. General adaptive filter scheme 4
Figure 2.3. FIR filter structure 4
Figure 2.4. Multistage lattice filter...5
Figure 2.5. Adaptive filter scheme for noise cancellation application.............................5
Figure 2.6. Adaptive filter scheme for unknown system identification...........................6
Figure 2.7. LMS algorithm..7
Figure 2.8. Block diagram of stage m in a lattice predictor 11
Figure 2.9. An example of white noise 12
Figure 2.10. Power spectrum of four types of colored noise 13
Figure 2.11. IoT-driven electronic stethoscope..14
Figure 2.12. Diaphragm and chest piece of the electronic stethoscope 14
Figure 2.13. 2D view of the electronic stethoscope 15
Figure 2.14. Electronic structure of the electronic stethoscope 15
Figure 2.15. Amplification circuit of the electronic stethoscope 16
Figure 2.16. Receiver device (NXP JN5169)..16
Figure 2.17. The electronic stethoscope circuit board 17
Figure 3.1. The test setup to collect auscultation data 18
Figure 3.2. Acoustic representation of the IoT-driven electronic stethoscope...............19
Figure 3.3. Electronic stethoscope system identification scheme..................................20
Figure 3.4. Example signals for *Channel* identification; **a)** input signal *x(n)*;
b) desired signal *d(n)*; error signal *e(n)* with *N* number of taps; **c)** *N*=8; **d)** *N*=16;
e) *N*=32; **f)** *N*=64; **g)** *N*=128; **h)** *N*=256 21
Figure 3.5. *Channel*'s estimated filter coefficients $wc(n)$..22
Figure 3.6. Example signals for identified *Channel* **a)** first microphone, *d(n)*;
b) second microphone, *x(n)*; **c)** zoomed output signal, *y(n)*, after converging 23
Figure 3.7. *Channel*'s magnitude response and phase response 23
Figure 3.8. The block diagram of ANC application...24
Figure 3.9. An example of generated synthetic data in Simulation 1 27
Figure 3.10. An example of generated synthetic data in Simulation 2 27
Figure 3.11. An example of generated synthetic data in Simulation 3 28

Figure 3.12. An example of generated synthetic data in Simulation 4 28
Figure 3.13. An example of real auscultation signal data 29
Figure 3.14. Signal processing steps 30
Figure 3.15. Signal processing step 1: ANC; **a)** the input signal *x(n)*; **b)** the desired signal *d(n)* and the output signal *e(n)*.. 30
Figure 3.16. Signal processing step 2 and 3: bandpass filtering and envelope generation; **a)** ANC application's output signal *e(n)*; **b)** filtered auscultation signal *s(n)* and its envelope signal $s_e(n)$.. 31
Figure 3.17. Signal processing step 2: power spectrum of the auscultation signal........ 31
Figure 3.18. Detected peaks in the auscultation signal 32
Figure 3.19. ROC curve 33
Figure 3.20. Detected bowel activities 34
Figure 3.21. A detected bowel activity with its temporal features................................ 34
Figure 4.1. MSE performance of adaptive filter algorithms for simulation 1................ 35
Figure 4.2. ANC application on synthetic data (simulation 1): an example of input signal and ANC outputs 39
Figure 4.3. ANC application on synthetic data (simulation 2): an example of input signal and ANC outputs 40
Figure 4.4. ANC application on synthetic data (simulation 2): an example of input signal and ANC outputs (a closer look at an IN) 41
Figure 4.5. ANC application on synthetic data (simulation 3): an example of input signal and ANC outputs 42
Figure 4.6. ANC application on synthetic data (simulation 3): an example of input signal and ANC outputs (a closer look at an IN) 43
Figure 4.7. ANC application on synthetic data (simulation 3): an example of input signal and ANC outputs (a closer look at a BS)... 44
Figure 4.8. ANC application on synthetic data (simulation 4): an example of input signal and ANC outputs 45
Figure 4.9. ANC application on synthetic data (simulation 4): an example of input signal and ANC outputs (a closer look at an IN) 46
Figure 4.10. ANC application on synthetic data (simulation 4): an example of input signal and ANC outputs (a closer look at a BS)... 47

Figure 4.11. ANC application on real auscultation data: an example of input signal and ANC outputs..48
Figure 4.12. ANC application on real auscultation data: an example of input signal and ANC outputs (a closer look at an IN)..49
Figure 4.13. ANC application on real auscultation data: an example of input signal and ANC outputs (a closer look at a BS)..50
Figure 4.14. An example of detected bowel activity while noise is absent 52
Figure 4.15. An example of detected bowel activity while noise exists 52
Figure 4.16. An example of detected bowel activity that coincides with the noise.......52

LIST OF TABLES

Table 2.1. Variable descriptions of LMS based algorithms 8
Table 2.2. Variable descriptions of the affine projection adaptive filter 9
Table 2.3. Variable descriptions of the RLS algorithm 10
Table 2.4. Variable descriptions of the adaptive lattice filter 11
Table 3.1. Average performances of adaptive filters for *Channel* identification 21
Table 3.2. Parameters of adaptive filter algorithms 25
Table 3.3. Signal parameters of synthetic data generation 26
Table 3.4. Synthetic data generation features 26
Table 3.5. Signal parameters of real bowel sound recordings 29
Table 4.1. Performance assessments of adaptive filter algorithms for simulation 1 36
Table 4.2. Performance assessments of adaptive filter algorithms for simulation 2 36
Table 4.3. Performance assessments of adaptive filter algorithms for simulation 3 37
Table 4.4. Performance assessments of adaptive filter algorithms for simulation 4 37
Table 4.5. Performance assessments of adaptive filters on real auscultation data 38
Table 4.6. Bowel activity detection performances for each auscultation 51

1. INTRODUCTION

Internet of Things (IoT) is enabling several applications ranging from the environment to healthcare (Al-Turjman et al. 2020; Ulusar et al. 2017). The main idea is the ubiquitous presence around us with a variety of things or objects that are connected to the Internet. A key application for the IoT-based technologies is wireless medical sensors, which aim to observe patients' health status remotely without intervening his/her daily life and perform early diagnosis of possible diseases. For this, researchers have been developing tiny sensors that can observe heartbeat, blood pressure, temperature, and so on, apply signal processing algorithms, and then share it through wireless connectivity with medical professionals. Wireless medical sensors are also an indispensable tool for patients with certain disabilities and accessibility issues by making remote monitoring possible and minimized the necessity of hospital visits. Also, they are beneficial for healthy and active people for monitoring their daily activities and well-being.

Auscultation is the typical mean of observing body sounds and is commonly used in clinical environments. The technology exists since the early 1800s, and despite all the improvements, the overall aim is to identify specific sounds within the body. With the advent of technology, IoT-driven bioacoustics sensors can be utilized for continuous monitoring. There are some studies in the literature that aims to use electronic stethoscopes for observing pulmonary, heart sound and intestinal sounds (Frank et al. 2016; Ou et al. 2016; Tang et al. 2010).

Bowel activity monitoring and detection is one of the applications in patient monitoring. Real time detection of bowel motility after major abdominal surgery has significant importance in the patients' healing process (Schroeder et al. 1991). Electronic stethoscopes are simple devices and they are typically designed for observing body sounds for short periods. In order to make them suitable for long-term monitoring, a detection algorithm for the sound type of interest is required. Various researchers have studied automatic and semi-automatic detection of intestinal sounds. Some techniques such as fractal dimension (Hadjileontiadis et al. 2003), wavelet decomposition (Hadjileontiadis 2005a, 2005b) , neural networks (Dimoulas et al. 2008), SVM classification (Yin et al. 2018) are used for short term intestinal sounds analysis. Other studies focused more subtle change detections observed over longer durations (Dimoulas et al. 2007; Emoto et al. 2013; Kim et al. 2011).

For long term bowel activity monitoring, another problem is the varying noise that exists at every level, and every location of our daily lives. Two types of noise require extra attention: ambient noise and body sounds. Some studies focused on signal de-noising and wavelet-based noise reduction (Dimoulas et al. 2006; Hadjileontiadis 2005a, 2005b). Jatupaiboon et al. developed an electronic stethoscope prototype with adaptive noise cancellation (Jatupaiboon et al. 2010). The proposed prototype acquires cardiac sounds and noises with two different microphones integrated into the stethoscope. LMS algorithm for adaptive filtering is applied. Jiao et al. proposed a gradient adaptive step size LMS algorithm, that uses two adaptive filters to estimate gradients more accurately, for biomedical applications (Jiao et al. 2013). Some researches utilized classification techniques such as Naive Bayesian, and Minimum Statistics and spectral subtraction for noise attenuation (Ulusar 2014).

A bowel activity monitoring system has been developed by our group. In our first version, we proposed a real-time bowel activity monitoring system that is a modified from conventional stethoscope (Ulusar et al. 2013). An electret microphone was placed inside the tube of a traditional stethoscope. Then, the amplified signal was digitized using a data acquisition card and transferred to a computer using wired communication. In our second study, we developed a custom design electronic stethoscope with two microphones to observe both bowel activity and ambient noise (Türk et al. 2015). Signals were digitized using data acquisition card, but data transfer was still realized with a wired connection that causes a limitation in patient mobilization. In our last study (Ulusar et al. 2019), we proposed an IoT-driven electronic stethoscope that utilizes two microphones to observe both bowel activity and ambient noise. A ZigBee module was used for signal digitization, signal processing, and wireless data transfer. A battery was added to the stethoscope that supports long term bowel activity monitoring up to 18 hours. The electronic stethoscope is designed as tiny as possible to enable mobilization.

In this study, a bowel activity detection algorithm with active noise cancelling feature was developed for our custom design IoT-driven electronic stethoscope developed in our previous studies. The focus of this study is to develop an effective active noise cancellation application by using both microphones of the electronic stethoscope. Experiments were conducted using both synthetic and real auscultation data. Five different adaptive filters were tested for active noise cancellation and an ideal adaptive filter algorithm was determined. Then, bowel activity detection algorithm was developed using real auscultation data. Active noise cancellation, bandpass filter, signal normalization and Hilbert transform techniques were applied for signal enhancement. Bowel sounds were detected by using an amplitude threshold value which is determined from the generated ROC curve. The algorithm was tested on ten different auscultation recordings, and a sensitivity of 95.09% and a specificity of 95.83% were obtained in bowel sound recognition.

2. LITERATURE REVIEW

2.1. Bowel Sound Characteristics

Bowel sounds (BS) refer to sounds produced within small and large intestine during digestion. They are typically characterized as a non-stationary short-time signal with explosive character and described as gurgling, rumbling, growling, and high-pitched. These sounds are occasionally contaminated by other artifacts such as heartbeat, movement, breathing, and environmental noise. Bowel sound occurs between 100 and 500 Hz and the duration of a single bowel activity (BA) is typically between 0.02 and 0.1 seconds. Sound level varies and correlates with the intensity and the location of the bowel movement. Bowel activity occurs approximately every 2-12 second in an irregular pattern (Dimoulas et al. 2008).

BSs are typically classified into two types: single burst (SB) and multiple bursts (MB) (Dimoulas et al. 2008; Ulusar 2014). Quiet period (QP) is a period when no bowel activity or noise exists. Figure 2.1 shows signals and their corresponding power spectrum under different cases. The first signal belongs to a quiet period and the second signal shows an example of noise. The third signal contains a SB signal and the fourth signal contains a MB signal.

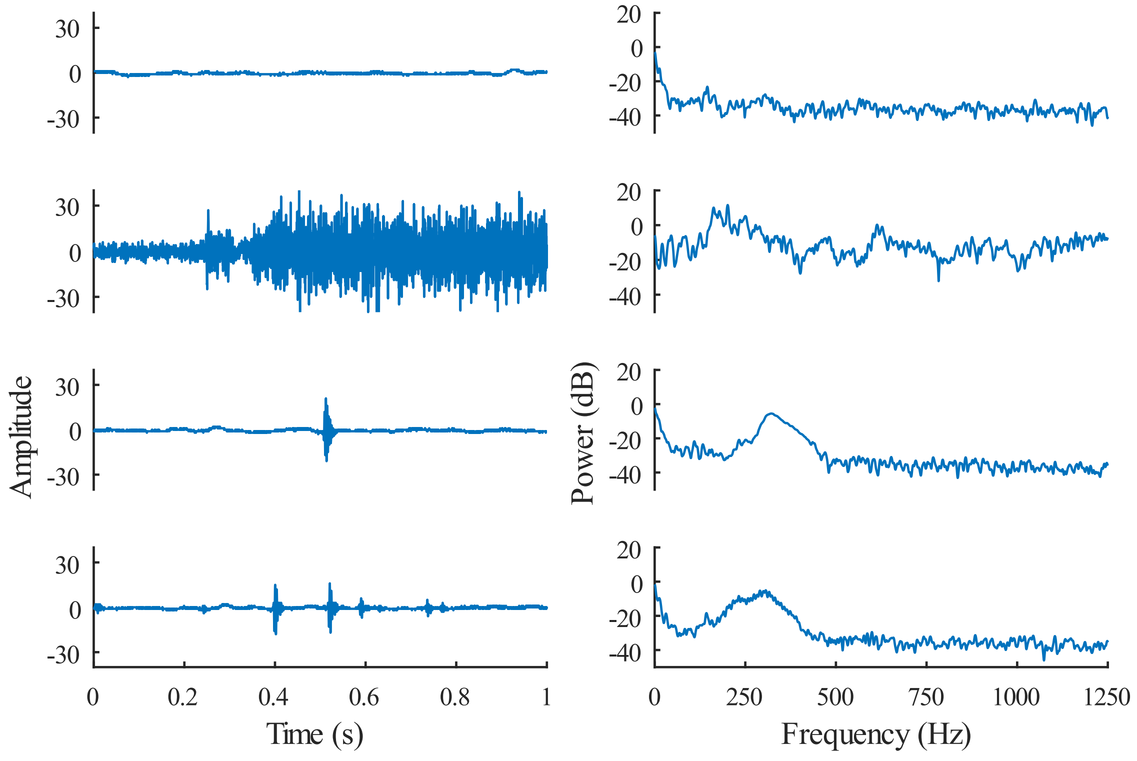

Figure 2.1. Auscultation samples under different cases (QP, Noise, SB, MB)

2.2. Adaptive Filters

Adaptive filters are digital filters whose coefficients change with an objective to make the filter converge to an optimal state. The optimization criterion is a cost function, which is most commonly the mean square of the error signal between the output of the adaptive filter and the desired signal. As the filter adapts its coefficients, the mean square error (MSE) converges to its minimal value. At this stage, the filter is adapted, and the coefficients have converged to a solution (Haykin 2013).

The block scheme of adaptive filtering environment is shown in Figure 2.2, where *n* is iteration number, *x(n)* donates input signal, *y(n)* is the adaptive filter output, and *d(n)* defines the desired signal. The error signal *e(n)* is calculated as *d(n)-y(n)*. Then, the error signal is utilized to form an objective function that used to update filter coefficients (Diniz 2020).

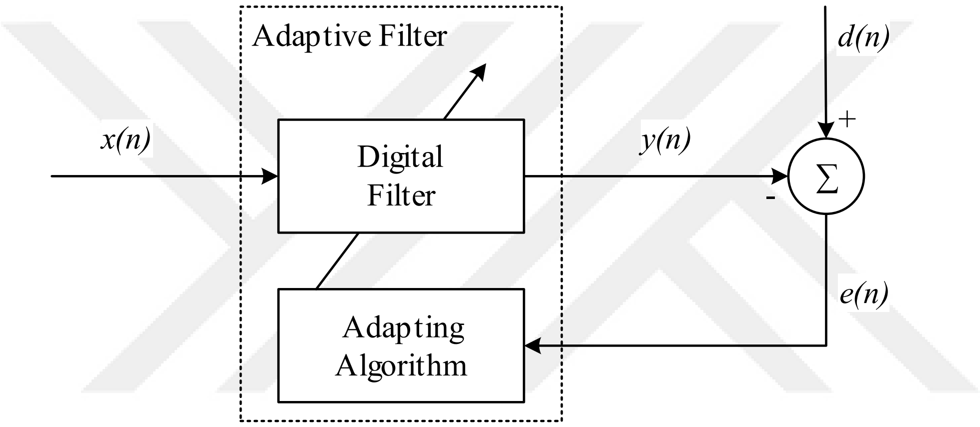

Figure 2.2. General adaptive filter scheme

As is shown in Figure 2.2, the structure of adaptive filter has two main substructures: a digital filter, and an adapting algorithm. Digital filter operates the input signal and produces an estimate of the desired signal. There are two types of filter structures mostly used in adaptive filtering: FIR filter, and lattice predictor. Structure of the FIR filter is given in Figure 2.3, and multistage lattice filter is shown in Figure 2.4.

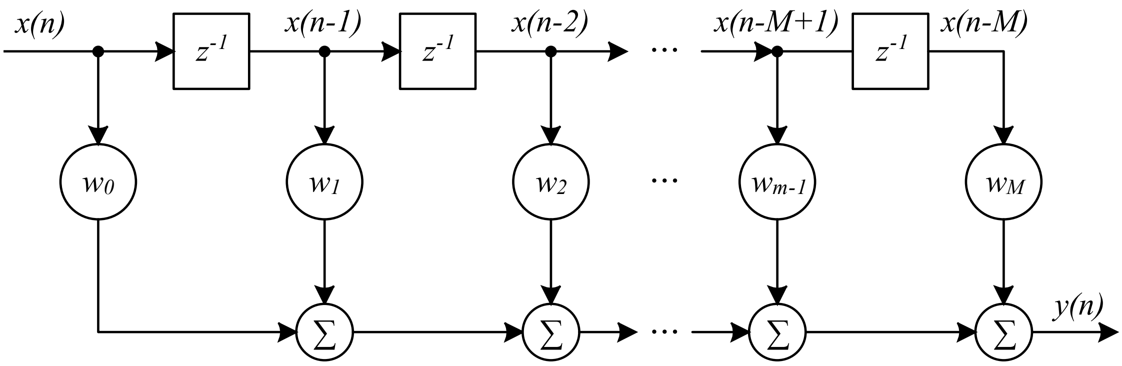

Figure 2.3. FIR filter structure

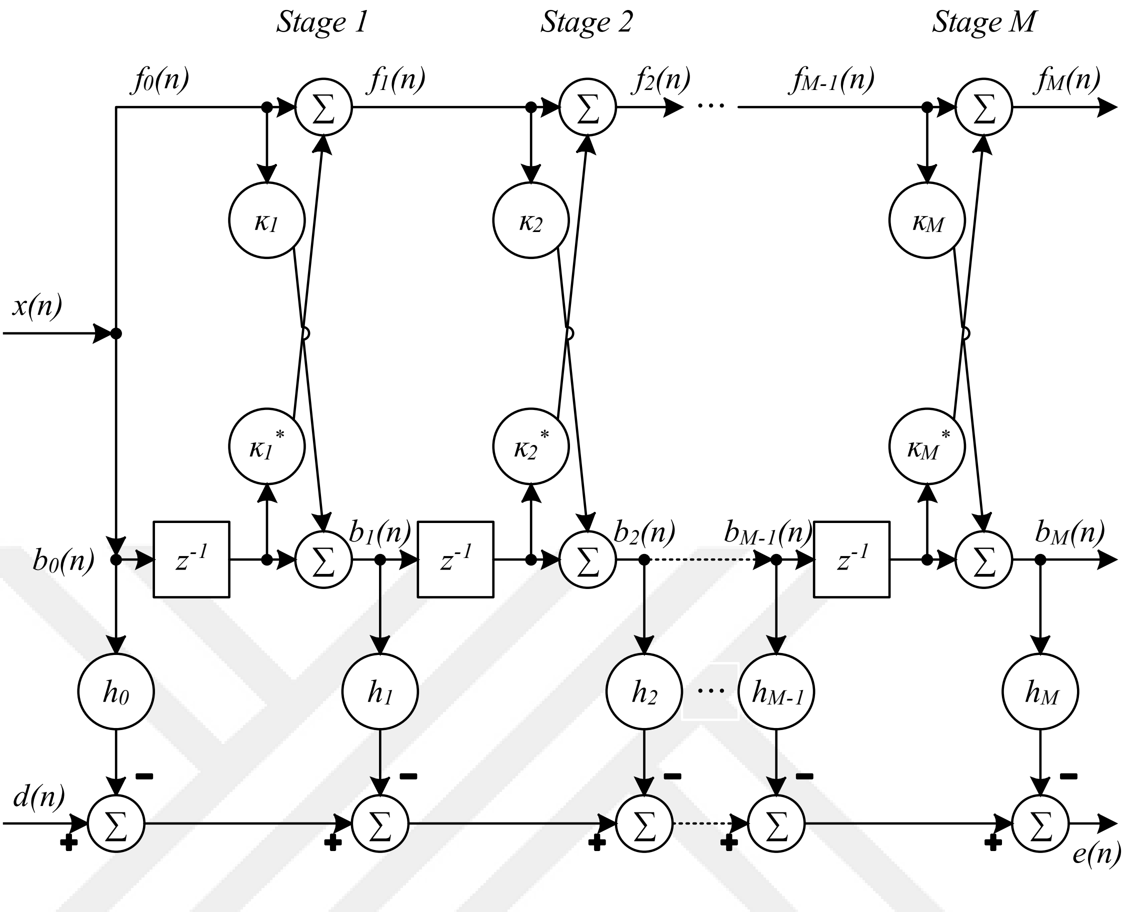

Figure 2.4. Multistage lattice filter

There are several applications of adaptive filters exists in signal processing. The application is selected by choice of the signals acquired from the environment. Adaptive filter applications are classified as identification, inverse modelling, prediction, and interference elimination, also known as noise cancellation (Haykin 2013).

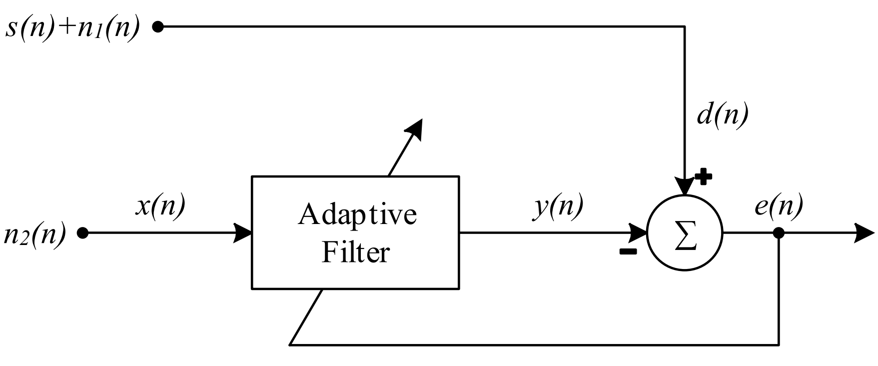

Figure 2.5. Adaptive filter scheme for noise cancellation application

In this thesis, the main idea to use an adaptive filter is noise or interference cancellation. In noise cancellation, the adaptive filter removes noise from a signal in real-time. Adaptive filter scheme for noise cancellation is shown in Figure 2.5. Here, the desired signal *d(n)*, the one to clean up, has noise and desired information. To remove the noise, feed a signal $n_2(n)$ to the adaptive filter that is correlated to the noise, $n_1(n)$, to be removed from the desired signal. As the input noise to the filter remains correlated to the unwanted noise accompanying the desired signal, the adaptive filter adjusts its coefficients to reduce the value of the error signal *e(n)* which is the difference between *y(n)* and *d(n)*, removing the noise and resulting in a clean signal in *e(n)*. The error signal converges to the signal *s(n)*, rather than converging to zero.

Unknown system identification is another adaptive filter application that is used in this study. Adaptive filters are used to identify an unknown system, such as the response of an unknown communications channel or the frequency response of an auditorium. In Figure 2.6, the unknown system is placed in parallel with the adaptive filter. This layout represents just one of many possible structures.

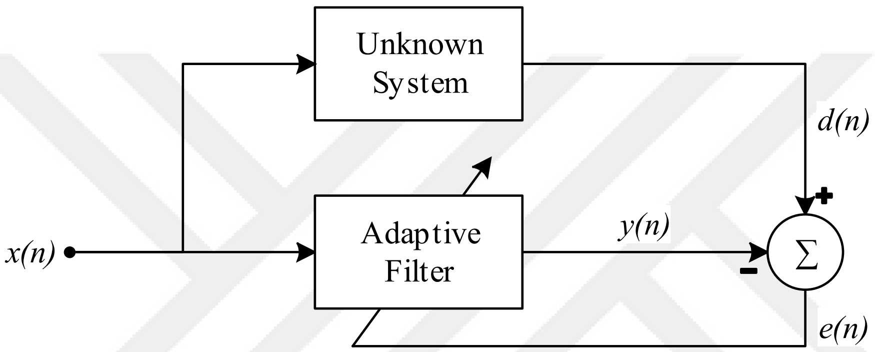

Figure 2.6. Adaptive filter scheme for unknown system identification

When the error signal *e(k)* is minimized, the adaptive filter response is close to the response of the unknown system. In this case, the same input feeds both the adaptive filter and the unknown.

There are many adaptive filter algorithms developed and selecting an algorithm for an application is a difficult task (Haykin 2013). The choice of one adaptive filter algorithm over another is determined by the following factors.

- **Rate of convergence:** This is also defined as the number of adaptation cycles required for the algorithm. A fast rate of convergence allows the algorithm to adapt rapidly to a stationary environment of unknown statistics.
- **Misadjustment:** This parameter provides a quantitative measure of the amount by which the final value of the mean-square error.
- **Tracking:** When an adaptive filtering algorithm operates in a nonstationary environment, the algorithm is required to track statistical variations in the environment.
- **Robustness:** For an adaptive filter to be robust, small disturbances can only result in small estimation errors. The disturbances may arise from a variety of factors, internal or external to the filter.
- **Computational requirements:** This refers to computational complexity, required buffer size, and the implementation complexity of the algorithm.

In this thesis, five different adaptive filter algorithms are selected and tested for active noise cancellation. In this section, the theoretical background of utilized adaptive filter algorithms is described.

2.2.1. The least-mean-square (LMS) algorithm

LMS algorithm is highly popular FIR based stochastic gradient descent application. It is easy to implement and computational complexity of the algorithm scales with the dimension of the FIR filter. The algorithm does not require any knowledge of statistical information of the environment.

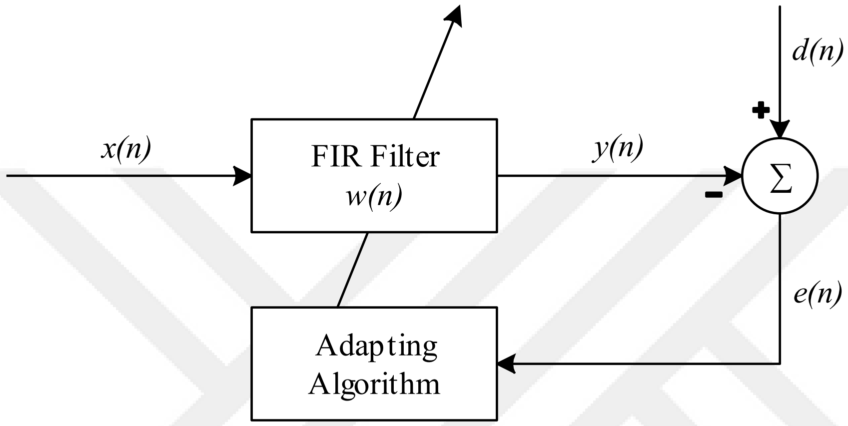

Figure 2.7. LMS algorithm

The structure of the LMS algorithm is shown in Figure 2.7. LMS algorithms have two fundamental processes. First, the filtering process that has two operations: computing output *y(n)* and generating estimation error by subtracting *y(n)* from *d(n)*. Second, the adaptation process that involves updating the present value of the estimated weight vector *w(n)*. LMS algorithm can be defined by the following equations (2.1) and variable descriptions are given in Table 2.1. In this algorithm, adaptive filter coefficients are updated using a step size parameter denoted by the input signal *x(n)* and the error signal *e(n)*.

$$0 < \mu < \frac{2}{\lambda_{max}}$$

$$y(n) = w^H(n-1)x(n) \tag{2.1}$$

$$e(n) = d(n) - y(n)$$

$$w(n+1) = w(n) + \mu x(n)e^*(n)$$

2.2.2. The normalized LMS (NLMS) algorithm

Various LMS adaptive filter algorithms have been developed. The main difference between these LMS based algorithms is the adapting function of the filter coefficients. In the traditional LMS algorithm, the adjustment applied to the tap-weight vector of the filter is directly proportional to the input vector *x(n)*. Therefore, when *x(n)* is too large, the LMS algorithm suffers from the gradient noise amplification problem. To overcome this problem, the normalized least mean square algorithm is developed. The error signal for the NLMS variant converges to zero much faster than the error signal for the LMS variant. The normalized version adapts in far less iterations to a result that is almost as good as the nonnormalized version.

In structural terms, the normalized LMS algorithm is same as the traditional LMS algorithm, as shown in Figure 2.7 . The NLMS algorithm is defined in the following equations (2.2), and variable descriptions are given in Table 2.1.

$$\begin{gathered} y(n) = w^H(n-1)x(n) \\ e(n) = d(n) - y(n) \\ w(n+1) = w(n) + \frac{\tilde{\mu}}{\|x(n)\|^2} x(n) e^*(n) \end{gathered} \tag{2.2}$$

Table 2.1. Variable descriptions of LMS based algorithms

Variable	Description
$x(n)$	The vector of buffered input samples at step n
$w(n)$	The vector of filter weight estimates at step n
$w^H(n)$	Hermitian transposition of w(n)
$y(n)$	The filtered output at step n
$e(n)$	The estimation error at step n
$e^*(n)$	The complex conjugate of e(n)
$d(n)$	The desired response at step n
$\tilde{\mu}$	The adaptation step size

2.2.3. Affine projection (AP) adaptive filter

The affine projection algorithm (AP) is an adaptive scheme that estimates an unknown system based on multiple input vectors. It is designed to improve the performance of other adaptive algorithms, mainly those that are LMS based. The affine projection algorithm reuses old data resulting in fast convergence when the input signal is highly correlated, leading to a family of algorithms that can make tradeoffs between computation complexity with convergence speed (Diniz 2020). AP adaptive filter is defined in the following equations (2.3), and variable descriptions are given in Table 2.2. In this set of equations, L is the length of input signal vectors.

$$X_{ap}^{T}(n) = \begin{pmatrix} x(n) & \cdots & x(n-L) \\ \vdots & \ddots & \vdots \\ x(n-N) & \cdots & x(n-L-N) \end{pmatrix} = [x(n) \quad \ldots \quad x(n-L)]$$

$$y_{ap}(n) = X_{ap}^{T}(n)w(n) = \begin{pmatrix} y(n) \\ \vdots \\ y(n-L) \end{pmatrix}$$

$$d_{ap}(n) = \begin{pmatrix} d(n) \\ \vdots \\ d(n-L) \end{pmatrix} \tag{2.3}$$

$$e_{ap}(n) = d_{ap}(n) - X_{ap}^{T}(n)w(n)$$

$$w(n+1) = w(n) + \mu X_{ap}(n)\left(X_{ap}^{T}(n)X_{ap}^{T}(n) + \gamma I\right)^{-1} e_{ap}(n)$$

Table 2.2. Variable descriptions of the affine projection adaptive filter

Variable	Description
$X_{ap}^{T}(n)$	Input signal vectors as matrix
$y_{ap}(n)$	Output signal vectors as matrix
$d_{ap}(n)$	Desired signal vectors as matrix
$e_{ap}(n)$	The error signal vectors as matrix
$w(n)$	The adaptive filter coefficients vector
μ	The adaptation step size

2.2.4. The recursive least-squares (RLS) algorithm

Least-squares algorithms aim to minimize the sum of the squares of the difference between the desired signal and the digital filter output. When new samples of the incoming signals are received at every iteration, the solution for the least-squares problem can be computed in recursive form resulting in the recursive least-squares (RLS) algorithms. The RLS algorithms convergence performance is fast when input signal correlation is high. These algorithms have competitive performance when working in a time-varying environment. Of course, all these advantages cause increased computational complexity (Diniz 2020; Haykin 2013).

Conventional RLS filter structure is the same as the standard LMS algorithm, as shown in Figure 2.7. The RLS algorithm is described in the following equations (2.4), and variable descriptions are given in Table 2.3.

$$\begin{gathered} y(n) = w^T(n-1)x(n) \\ e(n) = d(n) - y(n) \\ w(n) = w(n-1) + k(n)e(n) \\ k(n) = \frac{\lambda^{-1}P(n-1)x(n)}{1 + \lambda^{-1}x^H(n)P(n-1)x(n)} \\ P(n) = \lambda^{-1}P(n-1) - \lambda^{-1}k(n)x^H(n)P(n-1) \end{gathered} \tag{2.4}$$

Table 2.3. Variable descriptions of the RLS algorithm

Variable	Description
$x(n)$	The vector of buffered input samples at step n
$P(n)$	The inverse correlation matrix at step n
$k(n)$	The gain vector at step n
$w(n)$	The vector of filter taps estimates at step n
$y(n)$	The filtered output at step n
$e(n)$	The estimation error at step n
$d(n)$	The desired response at step n
λ	The forgetting factor

2.2.5. Adaptive lattice (AL) filter

The first method of stochastic gradient descent algorithm was the LMS algorithm. Another stochastic gradient descent based algorithm is the AL filter algorithm. Multistage lattice filter block diagram is shown in Figure 2.4. Also, Figure 2.8 shows a single stage of a multistage lattice predictor.

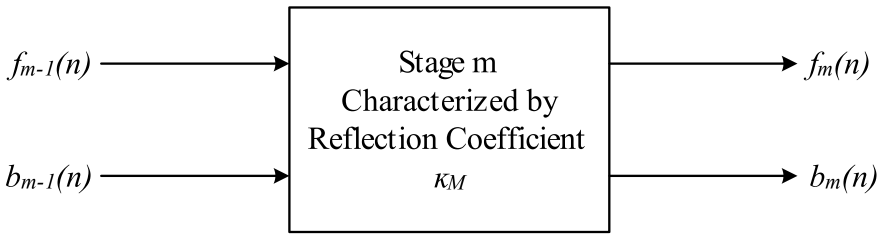

Figure 2.8. Block diagram of stage m in a lattice predictor

Unlike the LMS algorithm that is driven by the input signal directly, the adjustable tap weights in the AL algorithm are driven by the backward prediction errors produced by the multistage lattice predictor. Accordingly, there are two consecutive stages in the AL algorithm. Stage one involves recursive computation of the backward prediction errors, leading to recursive updates of the reflection coefficients. Stage 2 involves recursive update of the tap weights in the AL algorithm, followed by recursive estimates of the desired response (Haykin 2013). Desired response estimator of AL algorithm and update rule of lattice filter coefficients are given in the following equations (2.5), and variable descriptions are given in Table 2.4.

$$
\begin{aligned}
y_m(n) &= y_{m-1}(n) + h_m^*(n) b_m(n) \\
e_m(n) &= d(n) - y_m(n) \\
\|b_m(n)\|^2 &= \|b_{m-1}(n)\|^2 + |b_m(n)|^2 \\
h_m(n+1) &= h_m(n) + \frac{\tilde{\mu}}{\|b_m(n)\|^2} b_m(n) e_m^*(n)
\end{aligned}
\tag{2.5}
$$

Table 2.4. Variable descriptions of the adaptive lattice filter

Variable	Description
$f_m(n)$	Forward prediction error
$b_m(n)$	Backward prediction error
$e_m(n)$	Estimation error
$h_m(n)$	mth regression coefficient
$y_m(n)$	The estimation of desired response

2.3. Noise Modelling

In signal processing, noise is defined as any unwanted signal that interferes with communication, measurement, perception, or processing of an information-bearing signal. Noise is present in various degrees in almost all environments. There are several sources of noise: acoustic noise, electronic device noise, electromagnetic noise, electrostatic noise, transmission noise, co-channel interference and processing noise (Vaseghi 2008). Depending on noise's time characteristics, they are classified as impulsive noise and transient noise pulses. Impulsive noise consists of random short-duration noise pulses caused by mainly ambient noises. Transient noise pulses, observed in most communication systems, are burst of noise or long clicks caused by interference or damage to signals during storage or transmission.

Noises are classified as colors depending on their frequency spectrums. Different colors of noise have different properties. For example, they will sound different to human ears. Color names are given based on the power spectral density, $1/f^{\alpha}$, of the noise.

White noise is defined as an uncorrelated random noise process with equal power at all frequencies ($\alpha = 0$). A plot of the power spectrum of white noise shows flat shape as shown in Figure 2.9. In discrete time, white noise is a discrete signal whose samples are regarded as a sequence of serially uncorrelated random variables with zero mean and finite variance.

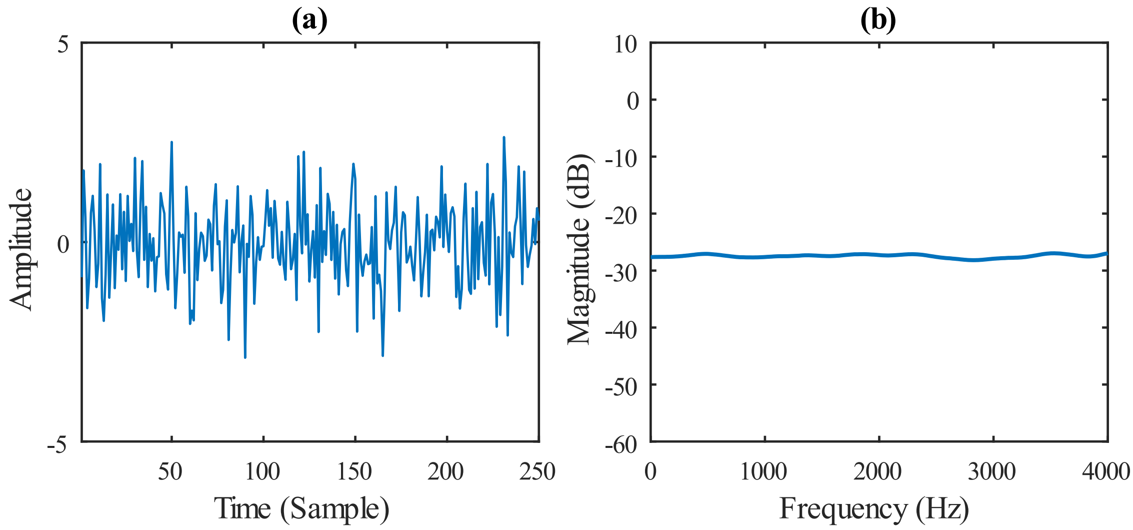

Figure 2.9. An example of white noise

Although the concept of white noise provides a reasonably realistic and mathematically convenient and useful approximation to most of the noises encountered in nature, many other noise processes are nonwhite. The term "colored noise" refers to any broadband noise with a nonwhite spectrum. There are four classic varieties of colored noise exist: pink noise, brown noise, blue noise, and purple noise. Power spectrums of these colored noises are shown in Figure 2.10.

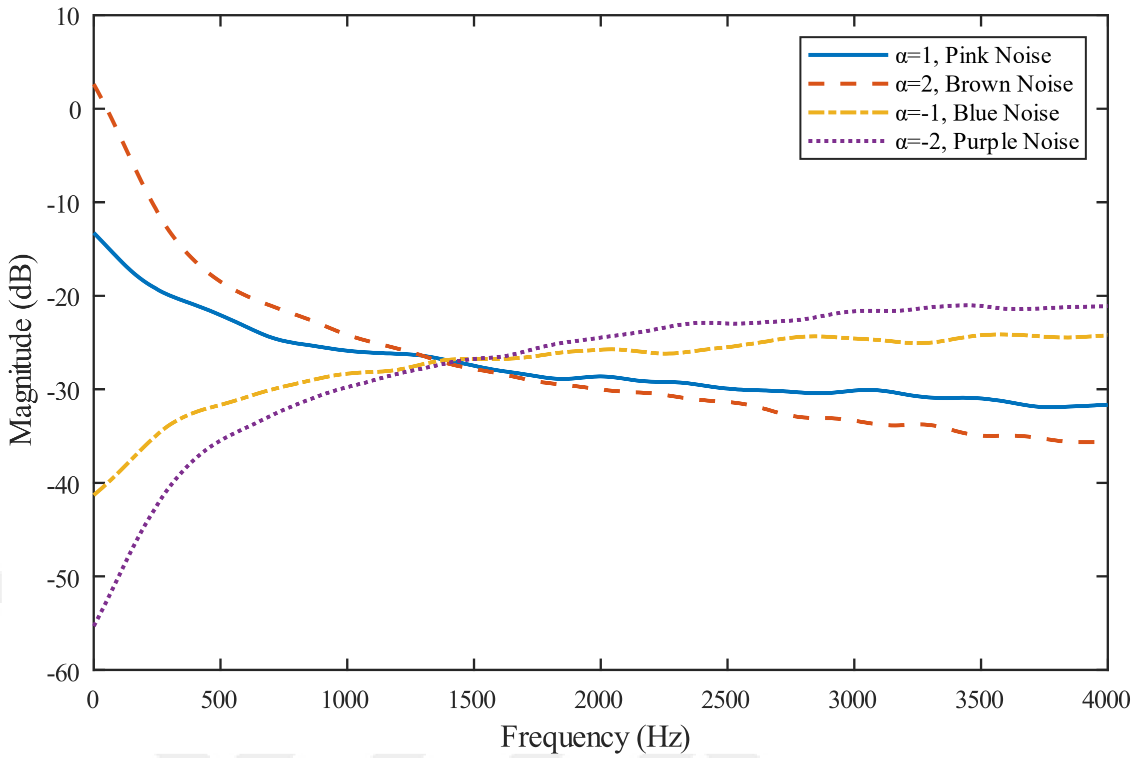

Figure 2.10. Power spectrum of four types of colored noise

Additive white Gaussian noise (AWGN) is a basic model to represent any random noise that occurs in nature. It provides a valid assumption and leads to a mathematically convenient and useful solution (Vaseghi 2008). The modifiers denote specific characteristics:

- **Additive:** The noise is additive because the channel consists of continuous electrical or processing noise.
- **White:** The noise is white because it is composed of all frequencies in the given range.
- **Gaussian:** The noise has a normal distribution in the time domain with an average value of zero.

The central limit theorem of probability theory indicates that the summation of many random noises will tend to have distribution called Gaussian or normal. AWGN is often used as a channel model. In this thesis, AWGN is used as a model to represent electrical noise for simulations and white Gaussian noise (WGN) model with the impulsive feature is selected as a model to represent ambient noise.

2.4. IoT-Driven Electronic Stethoscope

An IoT-driven wireless electronic stethoscope (Figure 2.11) was developed to collect, monitor, and detect bowel sound signals in our previous study (Türk et al. 2015; Ulusar 2014; Ulusar et al. 2019). The device consists of two main parts: mechanical structure and electronic hardware.

Figure 2.11. IoT-driven electronic stethoscope

In conventional stethoscopes, there is a part called chest piece, that has a circular shape, is used to listen to patients' body and picks up high-frequency sounds between 100 and 500 Hz (Hamlet et al. 1994). A custom stethoscope chest piece and diaphragm, shown in Figure 2.12, were designed and produced to be used in this electronic stethoscope.

Figure 2.12. Diaphragm and chest piece of the electronic stethoscope

2D view of the electronic stethoscope is shown in Figure 2.13. A covering box, made by 3D printer, is utilized to hold the electronic circuit, the battery, and the other equipment.

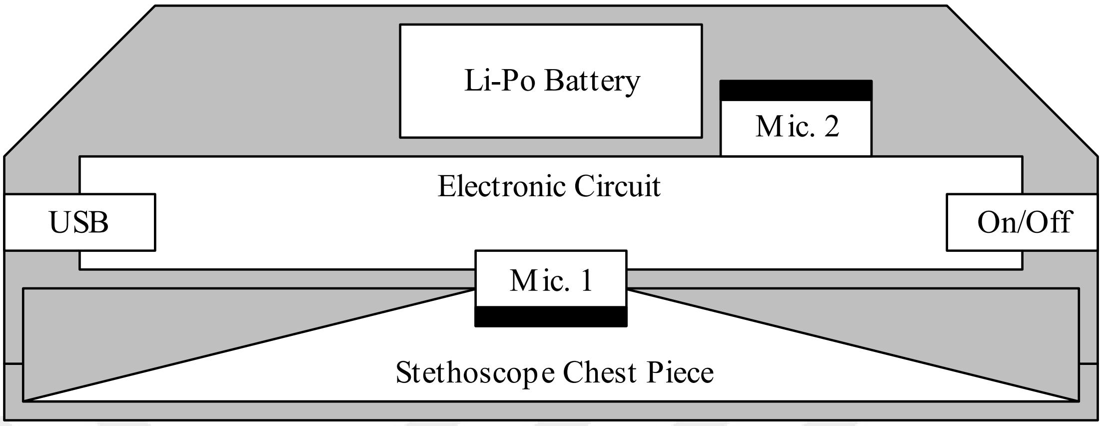

Figure 2.13. 2D view of the electronic stethoscope

Figure 2.14 shows the complete electronic architecture of the sensing device. Two electret microphones (POM-5246P-R, PUI Audio) were utilized to obtain sound signals. The first microphone, placed in the stethoscope's chest piece, listens to bowel signals while the second microphone, placed in the opposite direction, obtains environmental noise.

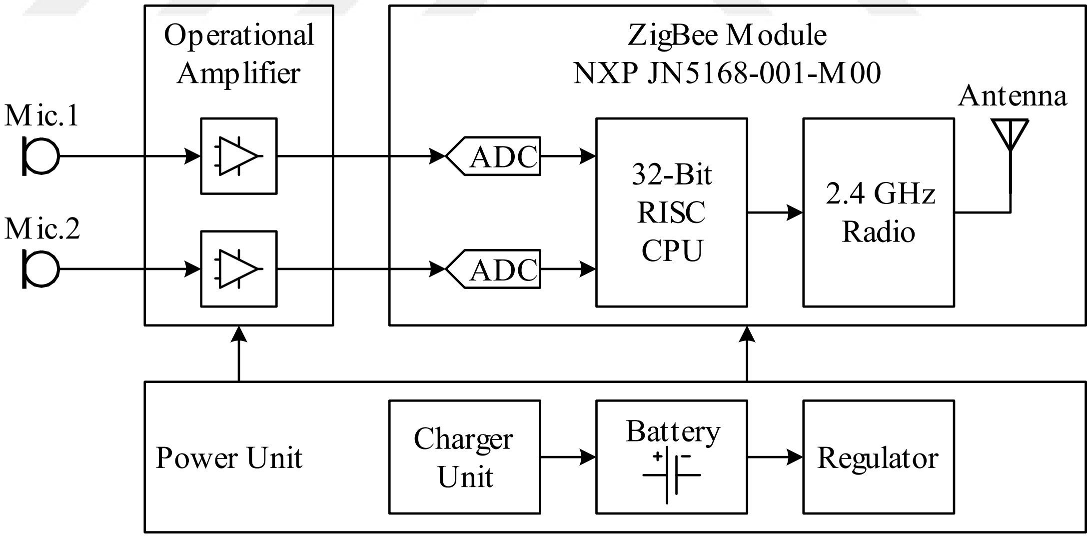

Figure 2.14. Electronic structure of the electronic stethoscope

The low amplitude signals acquired with the electret microphones are between 0 and 20 mV. Therefore, signals are amplified 48 times to increase the sensitivity using operational amplifier (LM358, Texas Instruments). Electret microphone and amplification circuit is shown in Figure 2.15.

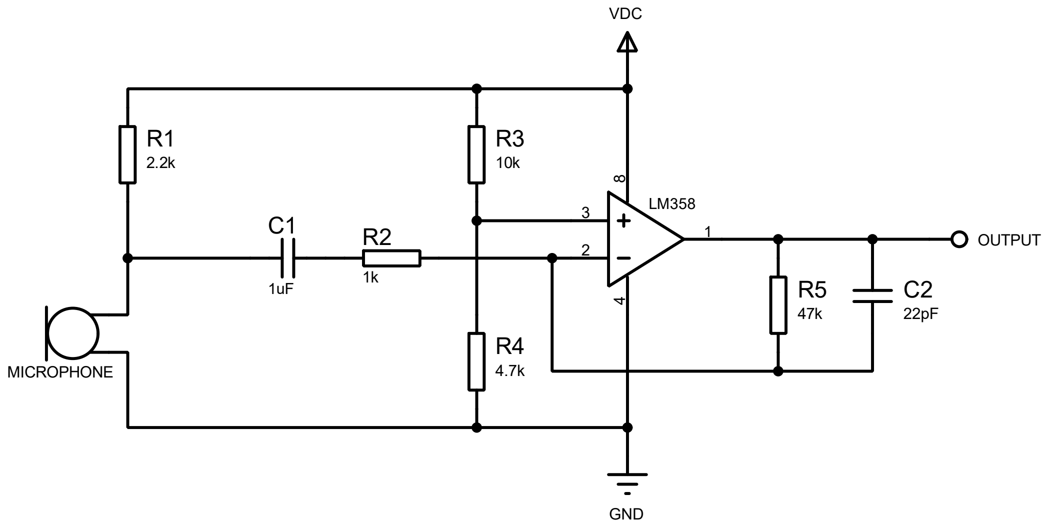

Figure 2.15. Amplification circuit of the electronic stethoscope

For wireless communication, there are many technologies exist such as Internet Protocol Version 6 (IPv6), Over Low Power Wireless Personal Area Networks (6LoWPAN), ZigBee, Bluetooth Low Energy (BLE), Z-Wave, Near Field Communication (NFC), etc. (Al-Sarawi et al. 2017). ZigBee communication technology has advantages for this specific application such as low power consumption, high data rate, and high communication range over other wireless communication technologies. ZigBee, based on the IEEE 802.15.4 protocol, operates at 2.4 GHz and suitable for short to mid-range IoT applications. It also offers high scalability, robustness, and high security.

ZigBee module JN5168 (NXP, Sheffield, UK) is used for ADC and wireless communication. It has a 32-bit RISC processor, 4-input 10-bit ADC, and consumes 0.12µA during deep sleep state and less than 25mA while communication state. Amplified signals are digitized using 10-bit ADC of the ZigBee module at a sampling frequency of 5 kHz. Buffered signals are transferred to the receiver device, JN5169 USB Dongle (Figure 2.16), connected to a computer.

Figure 2.16. Receiver device (NXP JN5169)

One cell lithium polymer battery (3.7V 380mAh) was used to power the system for up to 18 hours in the communication state. Battery charger circuit with micro USB interface was integrated into the system. Low noise voltage regulators (LP2985, Texas Instruments) were used separately to regulate input voltage for ZigBee module and operational amplifiers. Electronic stethoscope circuit board is shown in Figure 2.17.

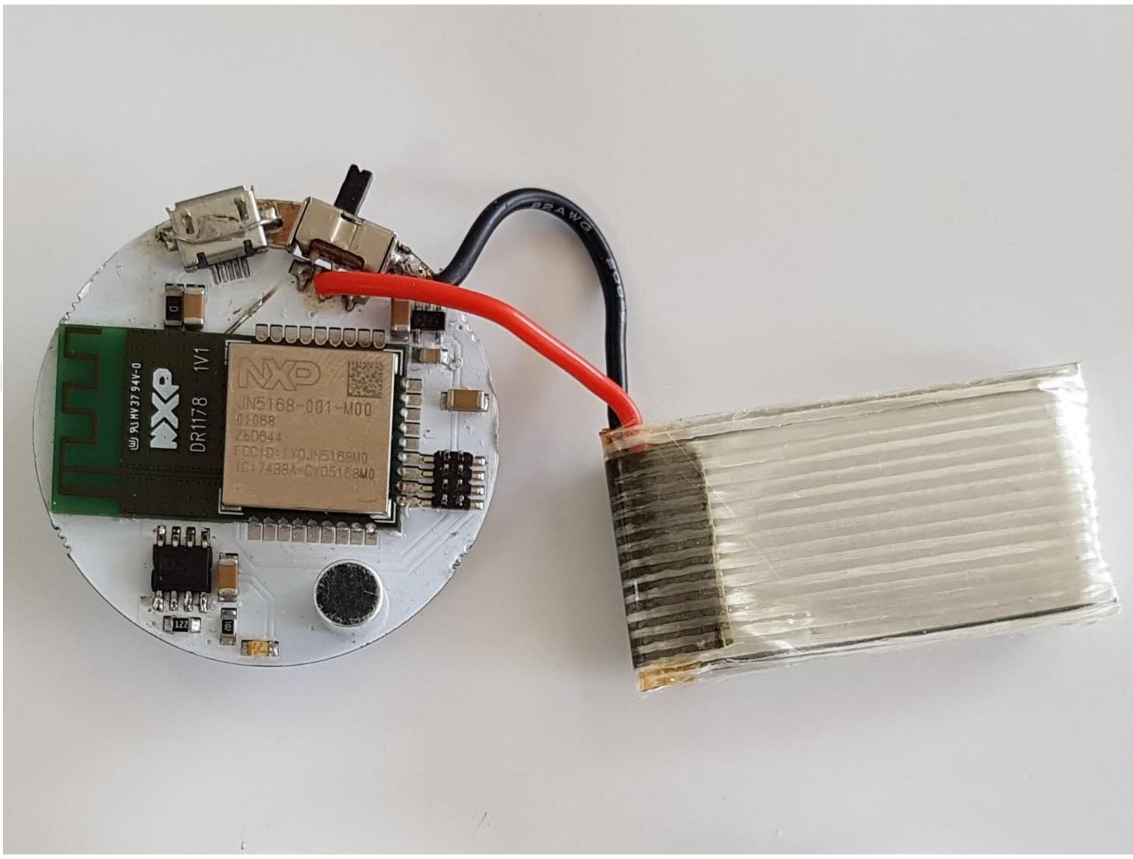

Figure 2.17. The electronic stethoscope circuit board

3. MATERIAL AND METHOD

The methodology of this thesis consists of two main sections. The first section describes adaptive filter algorithm determination for active noise cancellation (ANC), and the second section describes bowel activity detection algorithm. Developing an effective ANC application for the IoT-driven electronic stethoscope (Ulusar et al. 2019) is the focus of this study. ANC development was realized both using synthetic data and real auscultation data. Bowel activity detection algorithm was developed and tested using auscultation data labeled by an expert.

A test setup was built to collect auscultation data under a controlled environment, as shown in Figure 3.1. The setup consists of the custom design electronic stethoscope, a USB dongle (receiving device), a computer, and a speaker. The electronic stethoscope is placed on subject's abdomen and fixed with a medical patch tape. Signals are digitized at 5 kHz sampling frequency and transferred to the computer with 7-bit precision per channel. The speaker is placed 50 cm away from the electronic stethoscope and utilized to generate impulsive ambient noise. Impulsive noises are created using the white Gaussian noise model since it is a basic model to represent any random noise that occurs in nature (Vaseghi 2008).

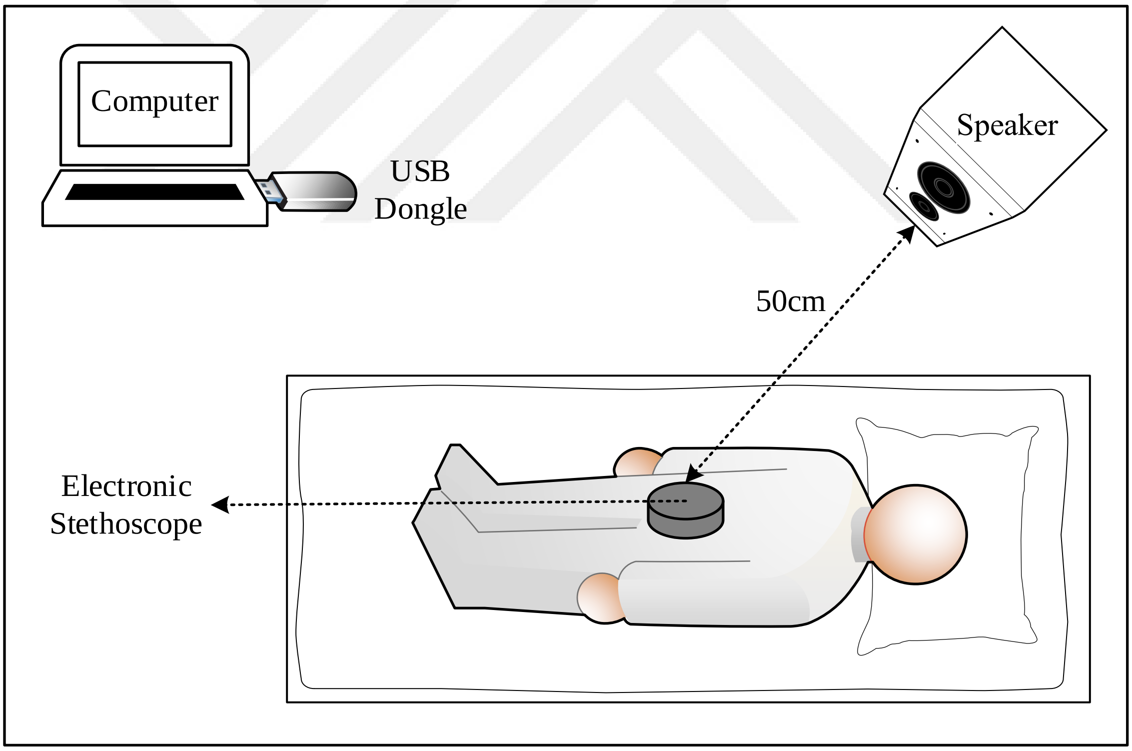

Figure 3.1. The test setup to collect auscultation data

3.1. Adaptive Filter Algorithm Determination for Active Noise Cancellation

The developed IoT-driven electronic stethoscope was equipped with two microphones, as shown in Figure 3.2. The first microphone (Mic. 1) is located inside the chest piece and used to observe only bowel sound signals. However, environmental noise often observed in the first microphone and causes false positive detection of bowel activity. Thus, a second microphone (Mic. 2) is utilized to observe only ambient noise and apply active noise cancellation. Due to the shape, orientation, and structure of the chest piece of the electronic stethoscope, the first microphone observes noise different than the second microphone.

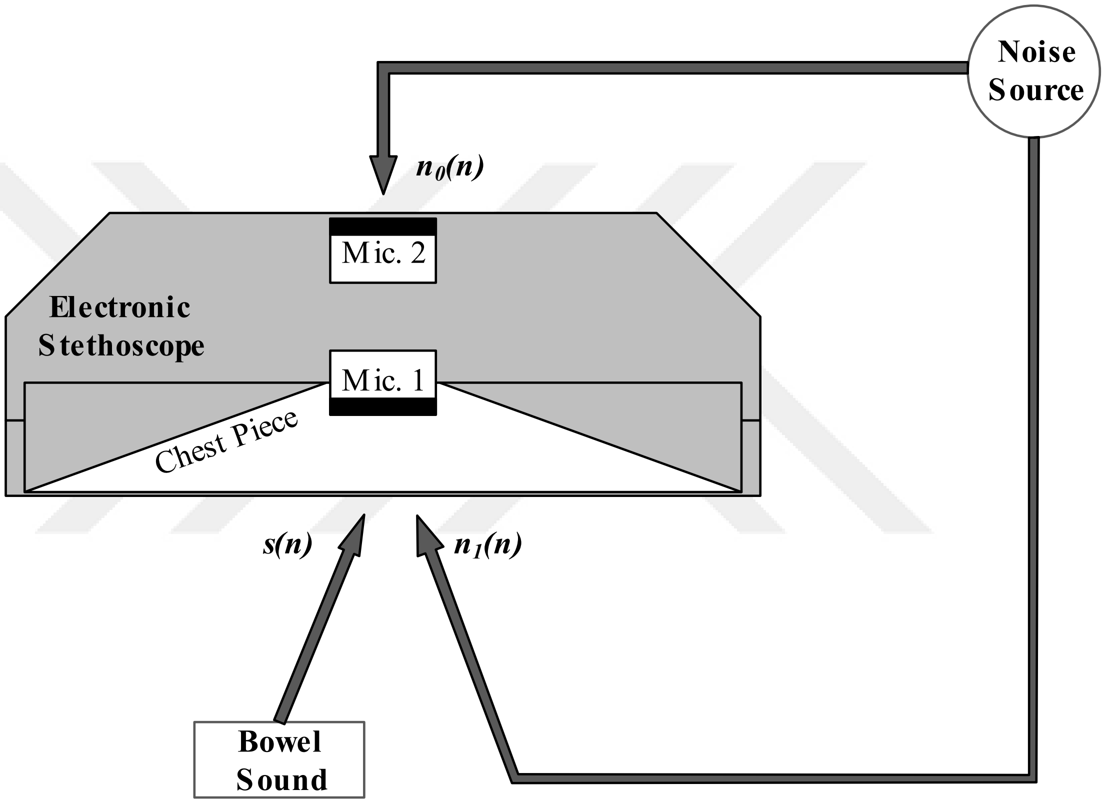

Figure 3.2. Acoustic representation of the IoT-driven electronic stethoscope

In this section, active noise cancellation experiments are realized using synthetic auscultation data and real auscultation data. Firstly, electronic stethoscope system is identified in order to generate synthetic data accurately. Then, application of active noise cancellation environment for the electronic stethoscope is explained. ANC performances of adaptive filters are compared, and an ideal adaptive filter is determined for our application.

3.1.1. Electronic stethoscope system identification

The first microphone observes noise different than the second microphone. This transformation is represented with the rectangle named *Channel* in Figure 3.3. In this section, *Channel*'s frequency response is identified to generate synthetic data for active noise cancellation applications.

In order to estimate the *Channel*'s properties, we used the RLS adaptive filter with the unknown system identification setting, as shown in Figure 3.3. The reason for using the RLS adaptive filter is its high performance and convergence rate over the other adaptive filters. Since the *Channel*'s identification is performed offline, the computational cost of the RLS algorithm, which is significantly higher than the other adaptive filters, is not a concern.

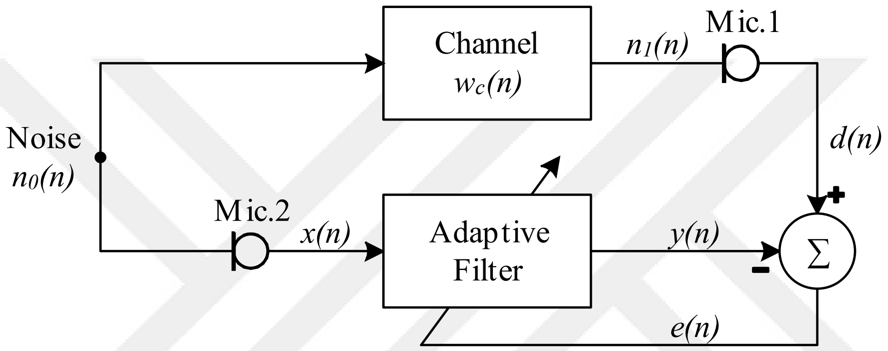

Figure 3.3. Electronic stethoscope system identification scheme

By using the test setup, 1-second long signals comprising 0.2-second long impulsive noises with the power of 20 dB are collected. In this case, ambient noise obtained with the second microphone $n_0(n)$ is used as the filter input *x(n)*, and altered ambient noise obtained with the first microphone $n_1(n)$ is used as the desired signal *d(n)*.

In order to discover the optimal response model, different lengths (8, 16, 32, 64, 128, 256) of FIR filters, called the number of taps, are tested in the RLS adaptive filter. 10 different signals are fed to the adaptive filters to acquire the average system model. When the error signal *e(n)* is minimized, the output signal *y(n)* is converged to the desired signal *d(n)*. Figure 3.4 shows an example of an input signal *x(n)*, desired signal *d(n)*, and converged error signal *e(n)* of each adaptive filter with different number of taps.

The power of error signal *e(n)*, the correlation between the output signal *y(n)* of the adaptive filter and the desired signal *d(n)*, and computation time are calculated to evaluate convergence success for each input data and filter length. The results are reported as mean value and standard deviation in Table 3.1. Lower power value and high correlation value mean more effective convergence.

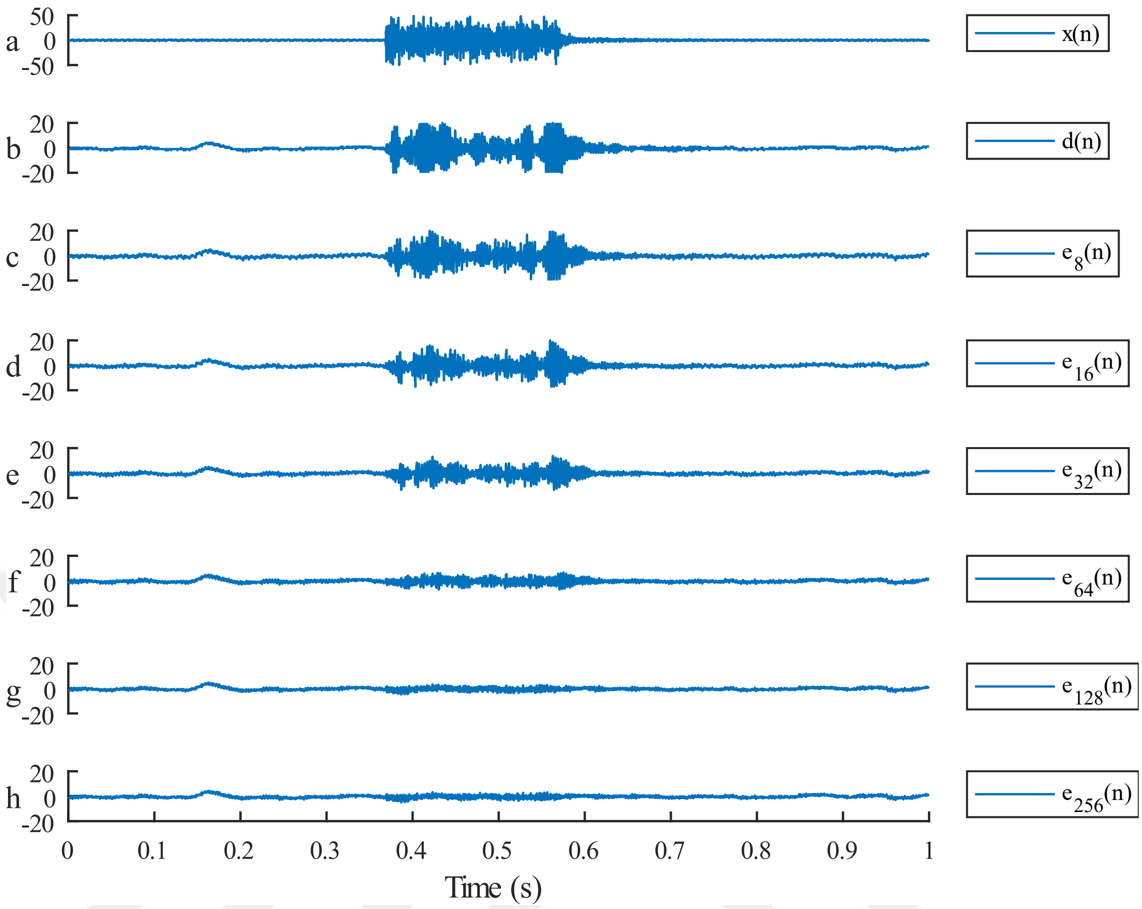

Figure 3.4. Example signals for *Channel* identification; **a)** input signal *x(n)*; **b)** desired signal *d(n)*; error signal *e(n)* with *N* number of taps; **c)** *N*=8; **d)** *N*=16; **e)** *N*=32; **f)** *N*=64; **g)** *N*=128; **h)** *N*=256

Table 3.1. Average performances of adaptive filters for *Channel* identification

Filter Length (N)	Computation Time t (s)		Power of Error Signal $P_{e(n)}$ (dB)		Correlation $Corr(y(n), d(n))$	
	μ	σ	μ	σ	μ	σ
8	0.0367	0.0035	9.0865	0.6128	0.6696	0.0237
16	0.0398	0.0040	7.3568	0.6298	0.7906	0.0189
32	0.0428	0.0043	4.8317	0.6827	0.8875	0.0131
64	0.0684	0.0049	1.7899	0.7969	0.9450	0.0088
128	0.2686	0.0192	0.6299	0.8502	0.9574	0.0079
256	0.4604	0.0299	0.5223	0.8156	0.9582	0.0078

It can be concluded from Table 3.1, the performance of adaptive filter increases as filter length increases. The adaptive filters with a length of 8, 16, 32, 64 show poor convergence performance. The adaptive filter with a length of 128 taps shows optimal performance since the average power of the error signal is lower than 1 dB and the correlation between its output and desired signal is more than 0.95. The adaptive filter with a length of 256 shows slightly better performance than the adaptive filter with a length of 128, but its computation time substantially higher than the others.

Estimated average FIR filter coefficients $w_c(n)$ are extracted for each filter with different tap numbers and shown in Figure 3.5. Besides, as shown in Figure 3.5/f, the coefficients after the tap number 128 are stable. Therefore, the FIR filter with a length of 128 is sufficient to model *Channel*.

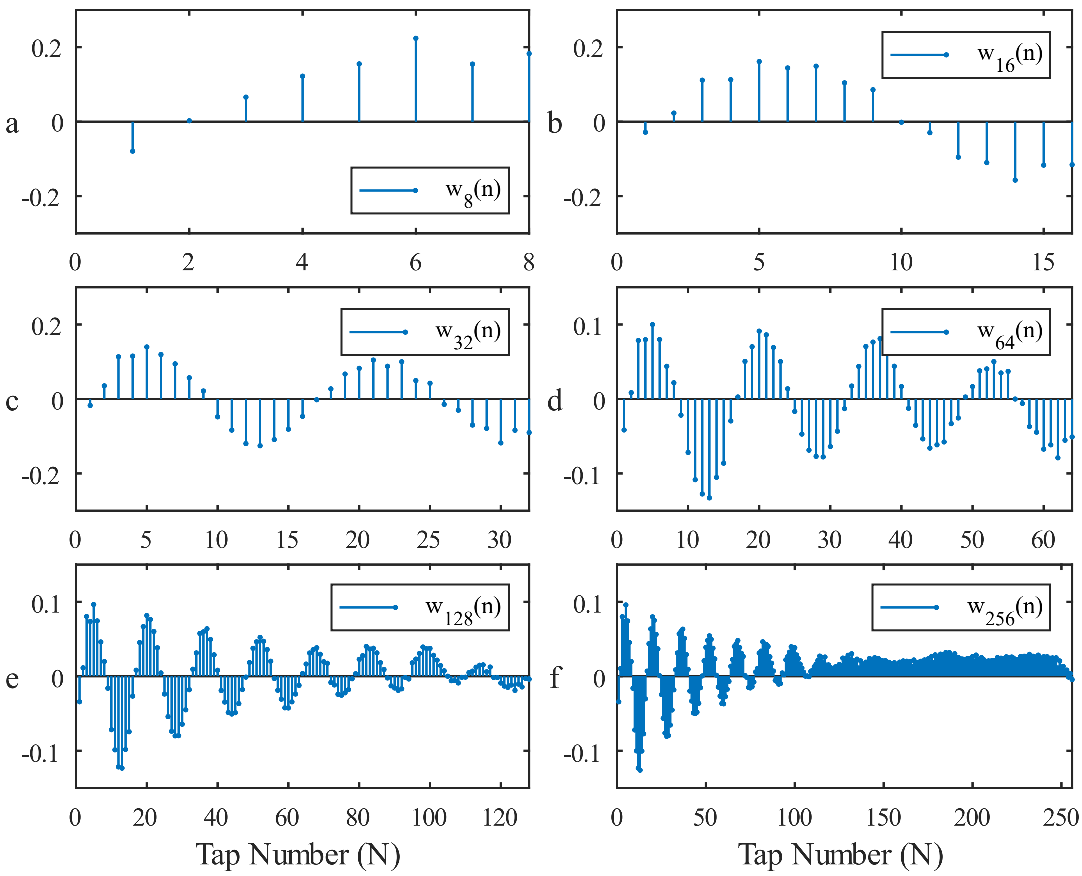

Figure 3.5. *Channel*'s estimated filter coefficients $w_c(n)$

As a result, the FIR filter with a length of 128 is selected to identify *Channel*'s frequency response since it has optimal computational cost and convergence success. Figure 3.6 shows an example of the desired signal *d(n)*, input signal *x(n)*, and a closer look at the comparison of the desired signal *d(n)* and adaptive filter's output *x(n)*.

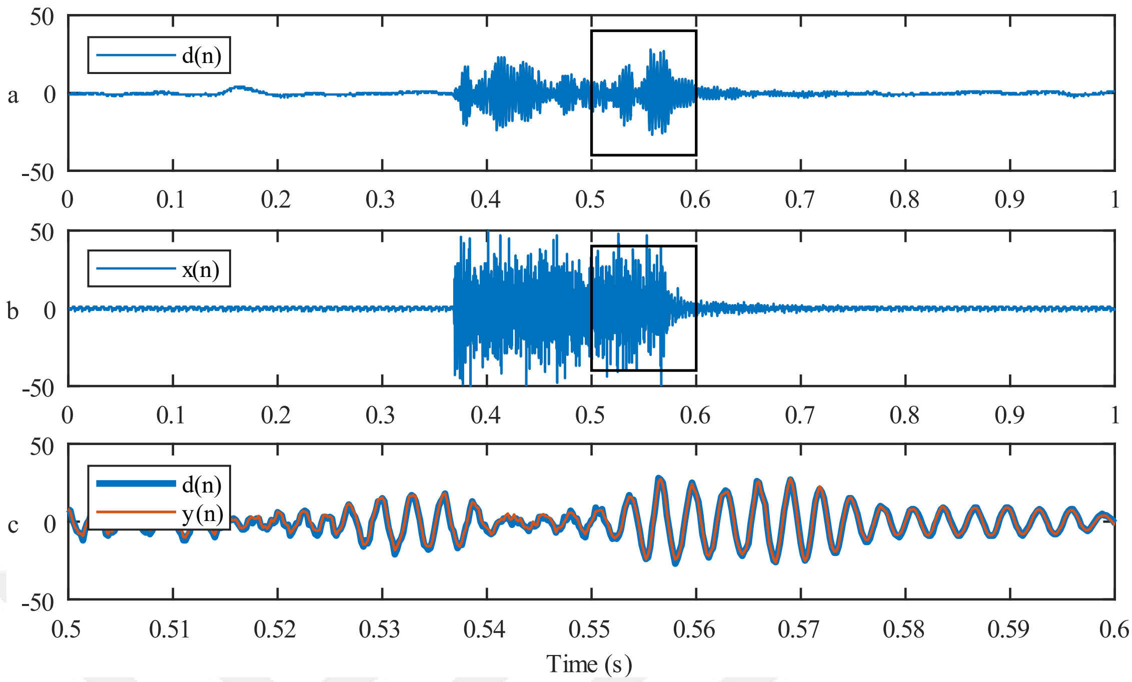

Figure 3.6. Example signals for identified *Channel* **a)** first microphone, *d(n)*; **b)** second microphone, *x(n)*; **c)** zoomed output signal, *y(n)*, after converging

Figure 3.7 shows the magnitude and the phase response of the *Channel*. The electronic stethoscope amplifies some signals up to 500 Hz and attenuates the rest. This frequency response is especially suitable for observing BSs and explains why bell-shaped chest pieces are used since bowel activity signals happen to be between 100 and 500 Hz. Ambient noise within the same frequency range passes through the stethoscope chest piece and is observed with the first microphone.

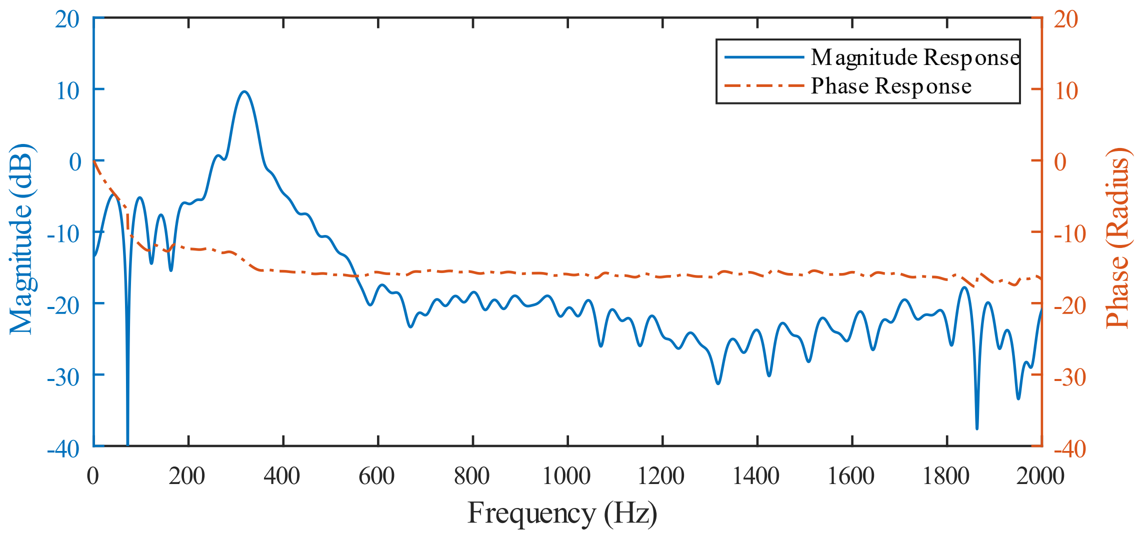

Figure 3.7. *Channel*’s magnitude response and phase response

3.1.2. Application of active noise cancellation

Figure 3.8 shows the block diagram of active noise cancellation for bowel activity detection. The first microphone, *Mic.1*, assigned as the desired signal *d(n)* and the second microphone, *Mic.2*, assigned as the input signal *x(n)* of the adaptive filter. *Channel* block represents the frequency response of the electronic stethoscope, which is identified in the previous chapter.

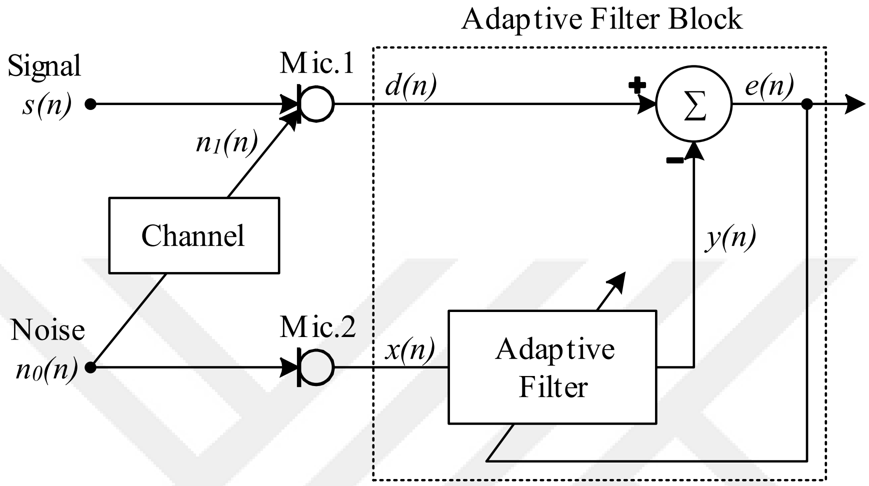

Figure 3.8. The block diagram of ANC application

Desired signal *d(n)* consists of bowel sound signals *s(n),* ambient noise $n_1(n)$ and electrical background noise $w_1(n)$ (3.1). Input signal *x(n)* consists of ambient noise $n_0(n)$ and background noise $w_0(n)$ (3.2). The ambient noise observed with the first microphone $n_1(n)$ is correlated with the ambient noise observed with the second microphone $n_0(n)$ (3.3). The background electrical noises are uncorrelated (3.4).

$$d(n) = s(n) + n_1(n) + w_1(n) \tag{3.1}$$

$$x(n) = n_0(n) + w_0(n) \tag{3.2}$$

$$n_1(n) = n_0(n)w_c(n) \tag{3.3}$$

The output signal of the adaptive filter *y(n)* is obtained by multiplying input signal *x(n)* with the adaptive filter coefficients *w(n)* (3.5). Adaptive filter adjusts its coefficients *w(n)* to reduce the value of the error signal *e(n)*, which is the difference between the desired signal *d(n)* and the output of the adaptive filter *y(n)* (3.6). Error signal *e(n)* is the output of the active noise cancellation application.

$$y(n) = x(n)w(n) \tag{3.5}$$

$$e(n) = d(n) - y(n) \tag{3.6}$$

In order to discover the most effective adaptive filter algorithm for our active noise cancellation application, five different adaptive filters are tested:

- The least-mean-square (LMS) algorithm
- The normalized LMS (NLMS) algorithm
- Affine projection (AP) adaptive filter
- The recursive least-squares (RLS) algorithm
- Adaptive Lattice (AL) filter

Based on empirical tests, adaptive filter parameters are optimized as in Table 3.2. As shown in Figure 3.8, error signal *e(n)* is the output of the ANC application. Performances of adaptive filters evaluated based on the MSE, computation time, the power of the output signal, and the correlation between desired signal and output signal.

Table 3.2. Parameters of adaptive filter algorithms

Symbol	**Parameter**	**Value**
N	Length of digital filter	128
μ_{LMS}	Adaptation step size of LMS algorithm	0.00003
μ_{NLMS}	Adaptation step size of NLMS algorithm	1
μ_{AP}	Adaptation step size of AP filter	1
L_{AP}	Projection order of AP filter	8
λ_{RLS}	Forgetting factor of RLS algorithm	1
λ_{AL}	Forgetting factor of AL filter algorithm	1

Selected adaptive filters are tested with two signals sets: synthetic auscultation data and real auscultation data. First, synthetic signal data set for both microphones is generated by using different simulations. Then, performances of the adaptive filters for each simulation are evaluated. Second, a real auscultation data set is collected and utilized to perform active noise cancellation application. Effectiveness of each adapting algorithm is analyzed and reported.

3.1.3. ANC application on synthetic auscultation data

Four different computer simulations are designed to generate a synthetic data set, and active noise cancellation is applied. In these simulations, signal parameters were determined based on the observations of real auscultation records taken with the developed electronic stethoscope (Table 3.3).

A single burst bowel sound signal extracted from real records was used as the BS signal. Ambient noise $n_0(n)$ is designed as zero-mean impulsive noise (IN) and generated using white Gaussian noise model. Altered ambient noise $n_1(n)$ is obtained by filtering original ambient noise $n_0(n)$ using FIR coefficients that represents electronic stethoscope frequency response. Finally, zero-mean additive white Gaussian noise is used as background noise (BN).

Table 3.3. Signal parameters of synthetic data generation

Symbol	Parameter	Value
f_s	Sampling frequency	5000 Hz
P_s	Power of BS signal	~20 dB
t_s	Duration of BS signal	0.04 s
P_n	Power of IN	20 dB
t_n	Duration of IN	0.2 s
P_w	Power of BN	-5 dB

Table 3.4 shows generated signal content for each simulation. These ANC simulations are performed 100 times, and in each of them, synthetic signal data is produced randomly. Performance results of ANC simulations are reported as mean and standard deviation value.

Table 3.4. Synthetic data generation features

	Duration (s)	Number of BS	Number of IN	$\boldsymbol{x(n)}$		$\boldsymbol{d(n)}$		
				$\boldsymbol{n_1(n)}$	$\boldsymbol{w_1(n)}$	$\boldsymbol{s(n)}$	$\boldsymbol{n_0(n)}$	$\boldsymbol{w_0(n)}$
1	0.2	0	1	+	-	-	+	-
2	60	0	10	+	+	-	+	+
3	60	30	10	+	+	+	+	+
4	60	30	10	+	-	+	+	-

Descriptions of four ANC simulations are as follows:

Simulation 1. ANC application with single IN

In this simulation, 0.2 seconds long input signal *x(n)* and desired signal *d(n)* are generated as shown in Figure 3.9. These signals consist of only a single IN. BN and BS signals are not used. Then, ANC applications using selected adaptive filters are performed. This simulation is performed to compare MSE performance of selected adaptive filter algorithms.

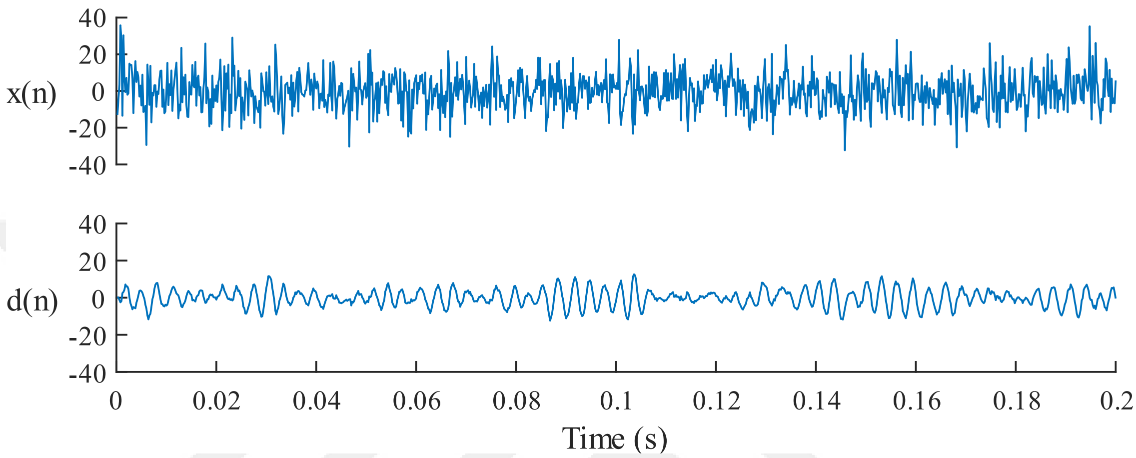

Figure 3.9. An example of generated synthetic data in Simulation 1

Simulation 2. ANC application with multiple IN

In this simulation, 60 seconds long input signal *x(n)* and desired signal *d(n)* are generated as shown in Figure 3.10. A dedicated number of INs are located randomly in the input signal and the desired signal. BN is added to final signals. Then, ANC applications using selected adaptive filters are performed. The purpose of this simulation is to compare adaptive filter performances against random INs where BSs are absent.

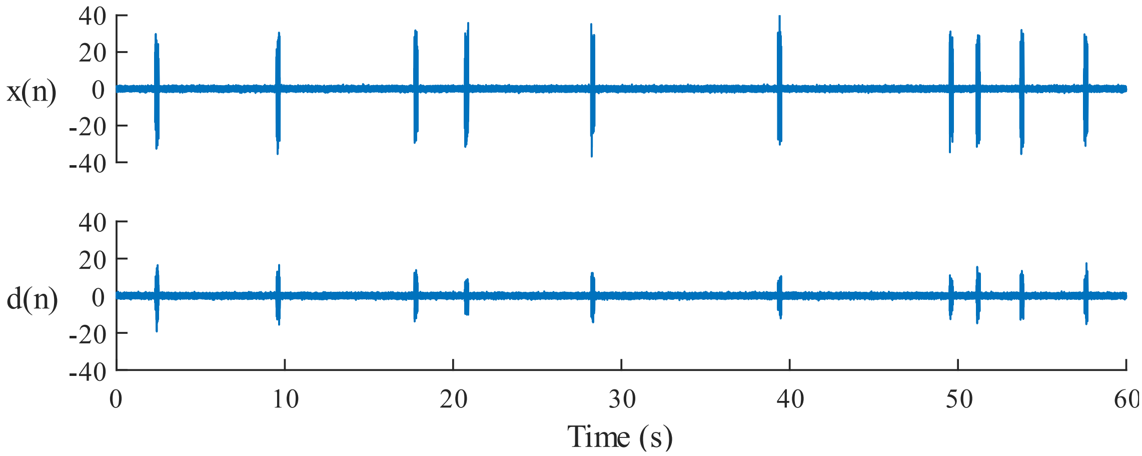

Figure 3.10. An example of generated synthetic data in Simulation 2

Simulation 3. ANC application with multiple IN and BS

In this simulation, 60 seconds input signal *x(n)* and desired signal *d(n)* are generated as shown in Figure 3.11. A dedicated number of INs and BSs are located randomly. BN is also added to final signals. Then, ANC applications using selected adaptive filters are performed. The purpose of this simulation is to compare filter performances against random INs where BSs exist and check if adaptive filters cause any corruption in BSs.

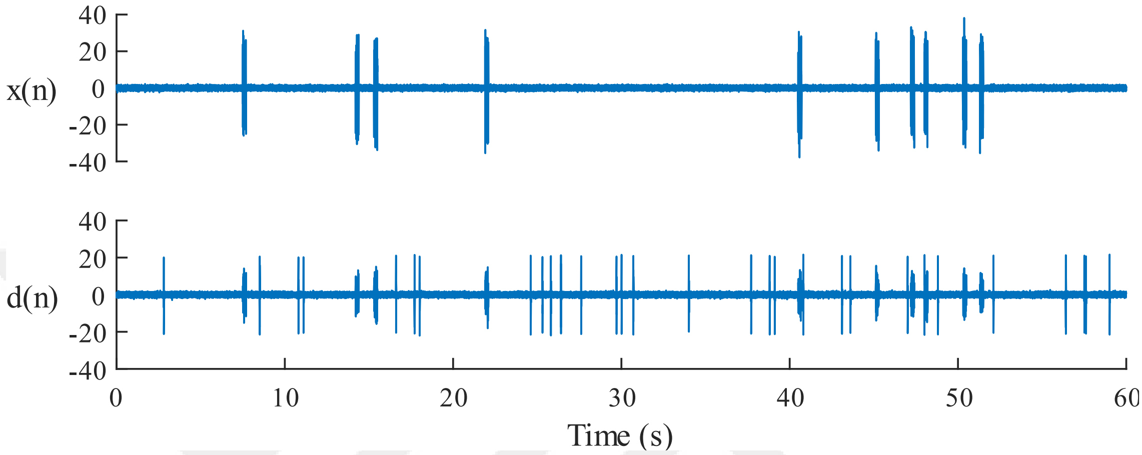

Figure 3.11. An example of generated synthetic data in Simulation 3

Simulation 4. ANC application with multiple IN and BS without BN

In this simulation, 60 seconds input signal *x(n)* and desired signal *d(n)* are generated as shown in Figure 3.12. A dedicated number of INs and BSs are located randomly. But BN is not used to calculate the correlation between BS signals and output of ANC application. The purpose of this simulation is to compare filter performances against random INs where BN is absent and check if adaptive filters cause any corruption in BSs.

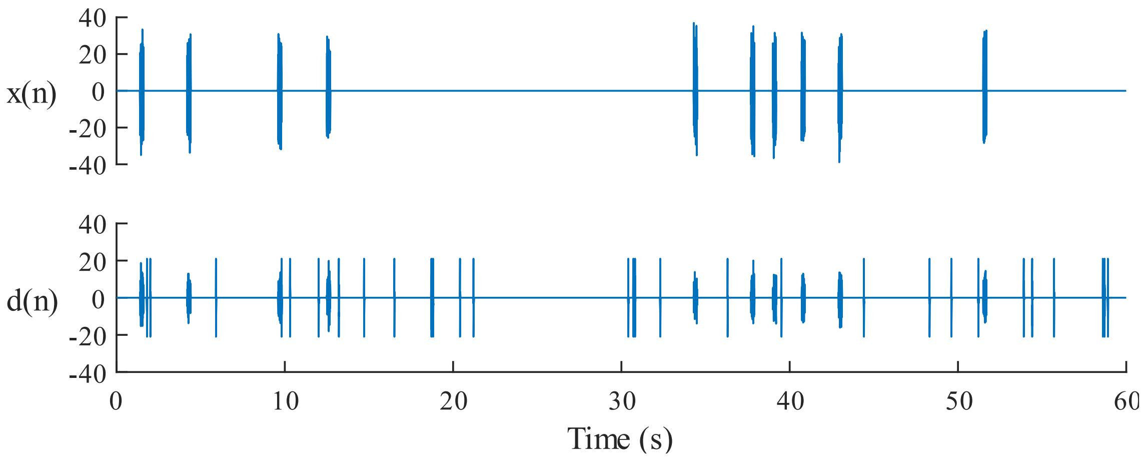

Figure 3.12. An example of generated synthetic data in Simulation 4

3.1.4. ANC application on real auscultation data

A dataset consisting of 10 auscultation recordings with a duration of 60 seconds was collected using the test setup. A dedicated number of ambient noises were randomly generated. Ambient noises designed as 0.2 seconds long INs and created with WGN model. Table 3.5 shows the parameters of auscultation recordings.

Table 3.5. Signal parameters of real bowel sound recordings

Symbol	Parameter	Value
N_r	Number of recordings in the dataset	10
T_r	Duration of each recording	60 s
f_s	Sampling frequency	5000 Hz
N_n	Number of INs in each recording	10
P_n	Power of an IN	20 dB
t_n	Duration of an IN	0.2 s

Figure 3.13 shows an example of recorded auscultation signal with the electronic stethoscope. Input signal *x(n)* shows the signal obtained with the second microphone and contains only ambient noises. The desired signal *d(n)* shows the signal obtained with the first microphone and consists of both INS and BSs. The occurrence of bowel sound signals cannot be controlled and depends on the subject’s intestinal motility.

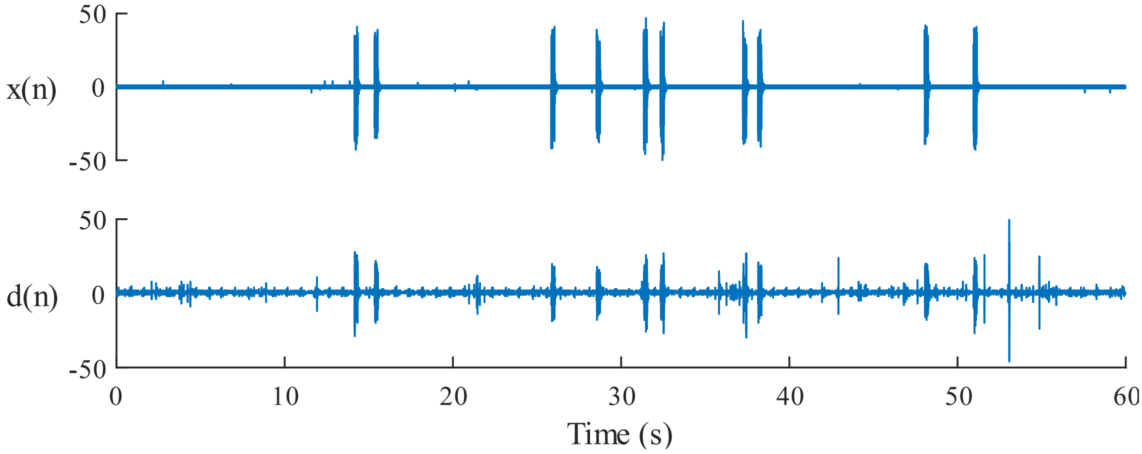

Figure 3.13. An example of real auscultation signal data

ANC was applied to each recording in the dataset by using selected adaptive filters. Performance results of ANC applications on real auscultation data are reported as mean and standard deviation value.

3.2. Bowel Activity Detection Algorithm

3.2.1. Signal processing steps

Several signal processing steps are applied to obtain clean auscultation signal as shown in Figure 3.14. Firstly, active noise cancellation is applied to remove ambient noise observed in both microphones. Then, a bandpass filter is used to remove unwanted information in the auscultation signal. Finally, envelope signal is obtained to simplify the auscultation signal. In order to explain signal processing steps, a two-second long auscultation piece, that contains an IN, BN and BS signals, is extracted from Figure 3.13 for the following illustrations.

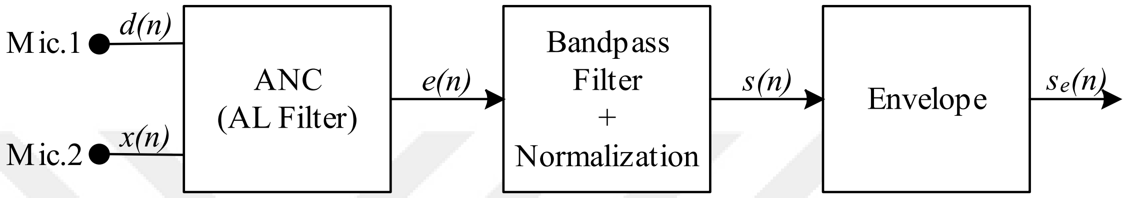

Figure 3.14. Signal processing steps

In the previous chapter, adaptive filter algorithms are compared based on their computational cost and noise reduction performances. AL filter is selected to be used in ANC application due to its high noise reduction performance and acceptable computation cost. Forgetting factor λ_{AL} of the AL filter is set to 1, and the filter length is set to 128. ANC application is performed to attenuate the interfering ambient noise observed in the first microphone. Figure 3.15.a shows the input signal *x(n)* that is acquired from the second microphone. Figure 3.15.b shows the desired signal *d(n)* and output signal *e(n)* of the ANC.

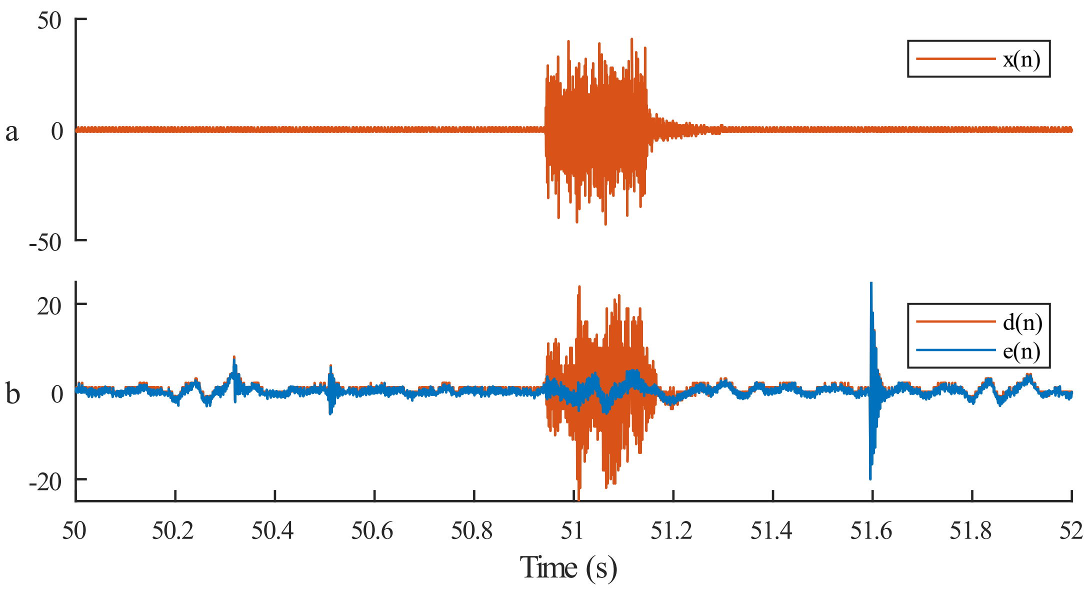

Figure 3.15. Signal processing step 1: ANC; **a)** the input signal *x(n)*; **b)** the desired signal *d(n)* and the output signal *e(n)*

Ambient noises are not the only unwanted signals that exist in the auscultation signal. A bandpass filter is applied to remove other known interferences such as inspiration, heartbeat, and power line. As is illustrated in Figure 3.16.b, ANC application's output signal *e(n)* is filtered from these interferences, and clearer auscultation signal *s(n)* is obtained. Since the frequency region of bowel sounds is between 100 and 500 Hz, the lower passband frequency is set at 100 Hz, higher passband frequency is set at 500 Hz, and stopband attenuation is set at 60 dB. Figure 3.17 shows the power spectrum of the auscultation signal before and after filtering.

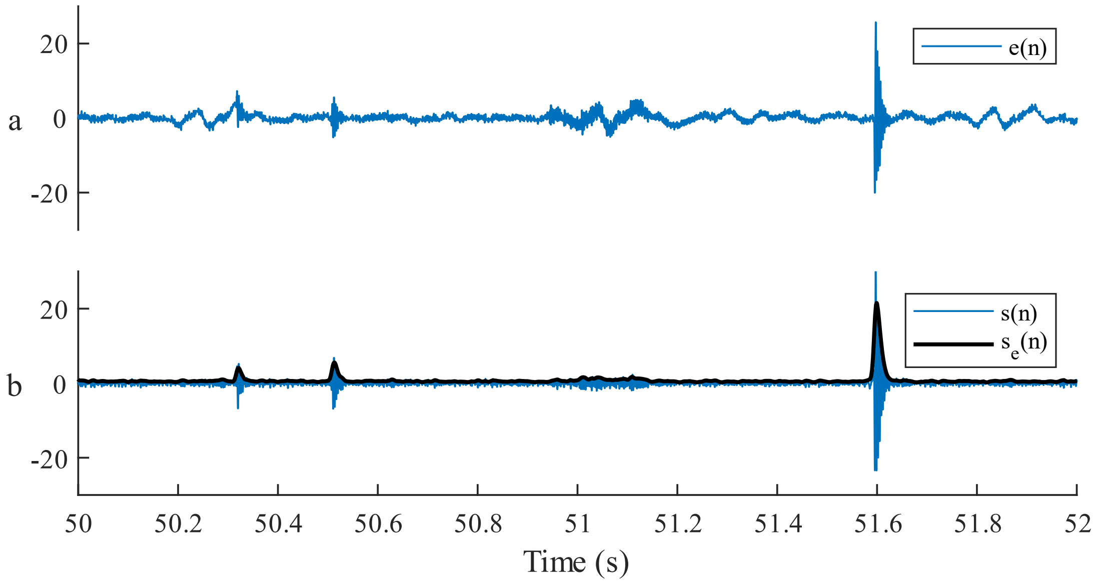

Figure 3.16. Signal processing step 2 and 3: bandpass filtering and envelope generation; **a)** ANC application's output signal *e(n)*; **b)** filtered auscultation signal *s(n)* and its envelope signal $s_e(n)$

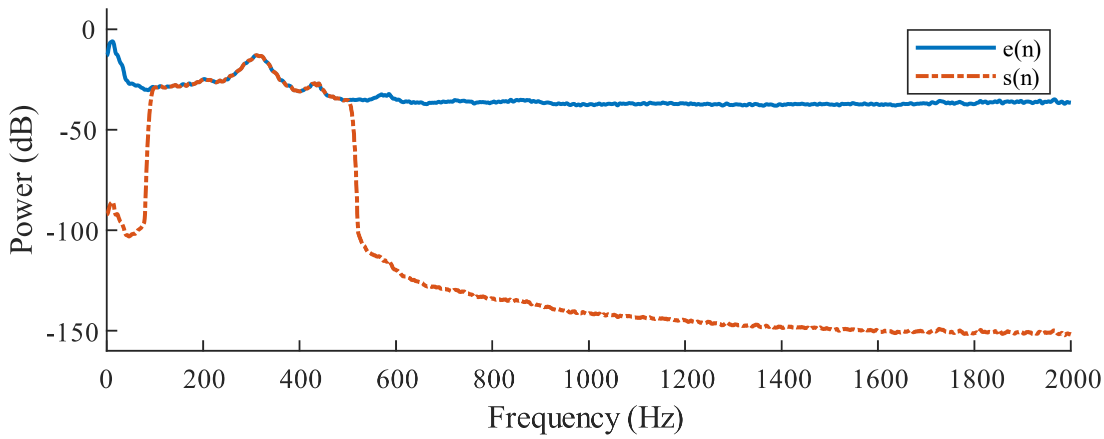

Figure 3.17. Signal processing step 2: power spectrum of the auscultation signal

The filtered auscultation signal is normalized by dividing signal to its standard deviation. Then, upper amplitude envelope signal $s_e(n)$ is generated using Hilbert transform, shown with back solid line in Figure 3.16.b.

3.2.2. Detection of bowel activity

The non-stationary character, variation on duration and amplitude of bowel activities make identification a very complex task. Auscultation signal *s(n)* was filtered using active noise cancellation and bandpass filters so far. The signal was then normalized by dividing the signal to its standard deviation. Standard deviation calculation is shown in the following equation (3.7).

$$\sigma_s = \sqrt{\frac{1}{L^2}\sum_{i=1}^{L}(s(i)-\bar{s})^2} \tag{3.7}$$

An envelope signal $s_e(n)$ of the zero-mean auscultation signal was extracted using Hilbert transform. However, background noise with the low amplitude values still exists in the signal. Signal's root mean square is commonly used to measure background noise and is also equal to the standard deviation of a zero-mean signal (Rizk et al. 2009).

Peaks on the envelope signal that have a higher amplitude value than the standard deviation were detected to identify bowel activities and noises. Figure 3.18 shows an example of detected peaks in the selected two seconds long auscultation. In this figure, bowel activities (156, 157, 161) and background noises (155, 158, 159, 160) can be observed clearly.

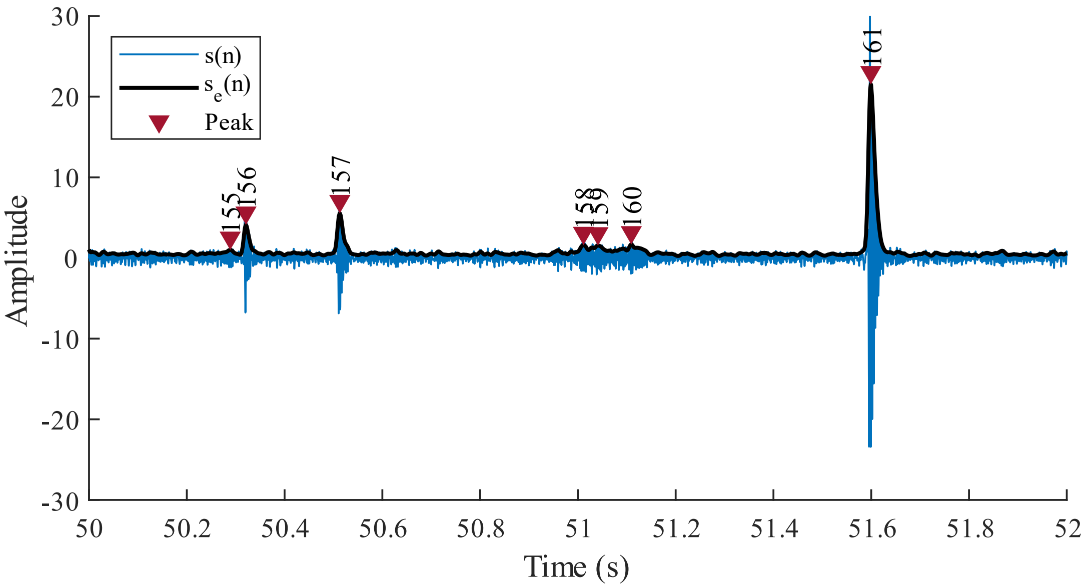

Figure 3.18. Detected peaks in the auscultation signal

In order to discriminate bowel activities from noises, an amplitude threshold value was determined by generating a ROC curve. Ten different 60 seconds long auscultation recordings were utilized to determine the amplitude threshold. The records were collected with the test setup and consists of randomly generated impulsive noises. An expert has labeled bowel activity regions belong to intestinal activities by both listening and observing auscultation signals. Then, each peak in the envelope signal was classified as BA or noise. 10 ROC curves were generated to observe classification performance for different threshold values.

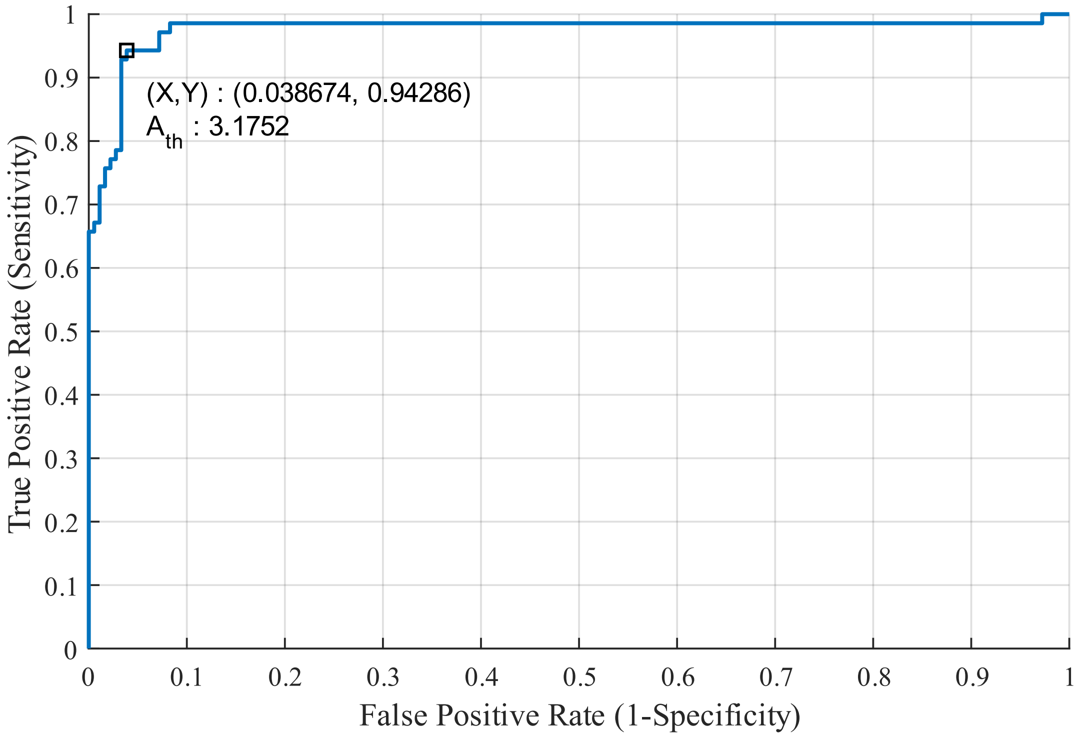

Figure 3.19. ROC curve

Figure 3.19 shows a ROC curve generated from a 60 seconds long auscultation recording. The optimum threshold value was determined by detecting the point on the curve that has the minimum distance to the ideal point (0,1) on the axis. The optimum threshold A_{th} value is identified as 3.1752 times the standard deviation.

Since the minimum bowel activity duration is 0.02 seconds, a duration threshold t_{th} value is also utilized to ignore peaks shorter than minimum bowel activity duration. A peak is classified as BA if its amplitude A_{BA} is higher than the amplitude threshold (3.8) and its duration t_{BA} is longer than the time threshold (3.9).

$$A_{BA} > A_{th} \tag{3.8}$$

$$t_{BA} > t_{th} \tag{3.9}$$

Figure 3.20 shows an example of detected bowel activity regions in the selected two seconds long auscultation. The dotted black line shows the amplitude threshold value. Orange signals indicate detected bowel activities and green triangles indicate the peak point of the bowel activity signals. Figure 3.21 shows a closer look at a single bowel activity that is detected in the same 60 seconds long signal.

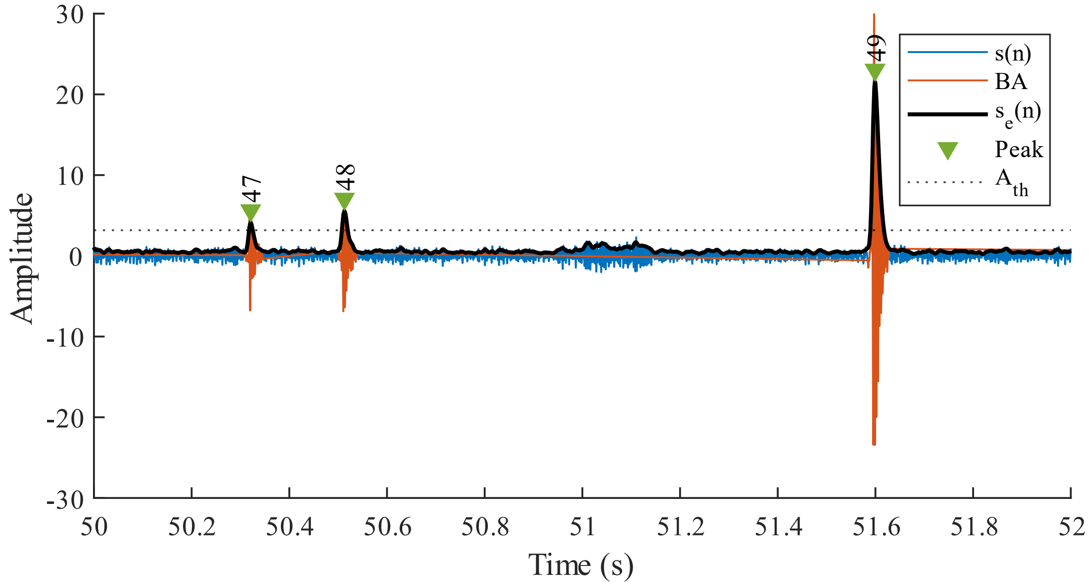

Figure 3.20. Detected bowel activities

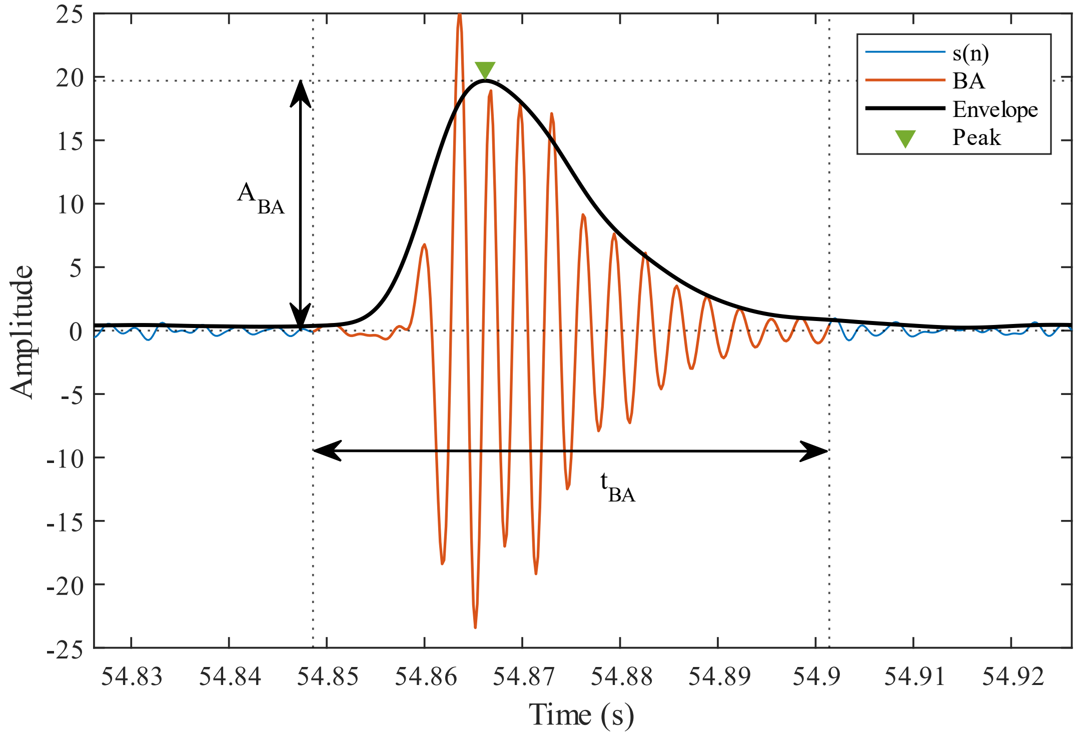

Figure 3.21. A detected bowel activity with its temporal features

4. RESULTS AND DISCUSSION

4.1. Results of Active Noise Cancellation Applications

Active noise cancellation applications were firstly performed on synthetic auscultation data. Then, a dataset of real auscultation data is used in the active noise cancellation applications. Performances of adaptive filters are reported in this section.

4.1.1. Results of ANC on synthetic auscultation data

Four different ANC simulation were designed to test ANC with different inputs. Each ANC simulation was performed 100 times to obtain accurate results. Performance results of adaptive filters are reported as mean values μ and standard deviation values σ.

In simulation 1, a single IN was generated, and output signals *e(n)* of selected adaptive filter algorithms were observed, as shown in Figure 4.2. MSE performances of adaptive filters are calculated. Figure 4.1 shows the average MSE signal obtained after 100 simulations. RLS and AL algorithms reached the minimum MSE value after 150 samples where NLMS and AP algorithms reached around 500 and LMS reached around 1000.

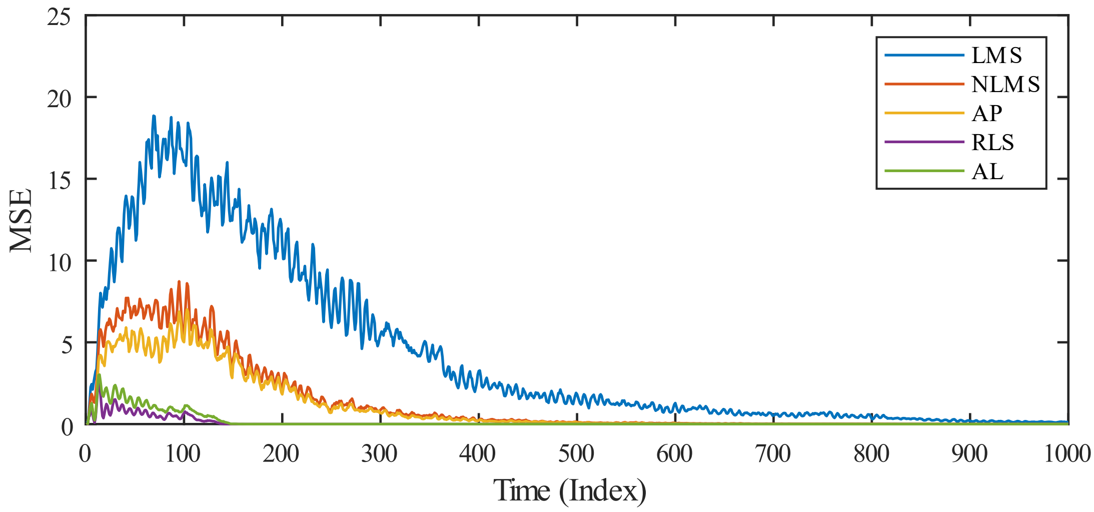

Figure 4.1. MSE performance of adaptive filter algorithms for simulation 1

Power and standard deviation of the average MSE signals were calculated and utilized for evaluation (Table 4.1). The lower standard deviation value of the MSE signal means faster convergence. According to simulation results, RLS and AL adaptive filters converge faster than other adaptive filters. RLS filter has a higher computational cost than AL filter, although its performance is better.

Table 4.1. Performance assessments of adaptive filter algorithms for simulation 1

Adapting Algorithm	Computation Time (s) t		Average MSE (dB)	
	μ	σ	P_{MSE}	σ_{MSE}
LMS	0.0248	0.0372	16.2237	4.9100
NLMS	0.0209	0.0055	8.0090	2.1511
AP	0.2350	0.0386	5.6985	1.6476
RLS	0.4716	0.0802	-11.1466	0.2640
AL	0.1809	0.0293	-6.5609	0.4442

In simulation 2, multiple INs were generated, and outputs of active noise cancellation algorithms were obtained, as shown in Figure 4.2. Figure 4.3 shows a closer look at the last IN in the data shown in Figure 4.2. The average value and the standard deviation of the power of output signals *e(n)* were calculated and utilized for evaluation (Table 4.2). LMS and AL algorithm attenuates ambient noise effects the most, among others.

Table 4.2. Performance assessments of adaptive filter algorithms for simulation 2

Adapting Algorithm	Computation Time (s) t		Power of Error Signal (dB) $P_{e(n)}$	
	μ	σ	μ	σ
LMS	0.0270	0.0019	-3.9845	0.0758
NLMS	0.0332	0.0016	0.0056	0.1334
AP	5.6195	0.0954	-0.0245	0.1222
RLS	13.0457	0.5606	-3.4346	0.2039
AL	2.3526	0.0440	-3.9927	0.0527

In simulation 3, multiple INs and BSs were generated, and outputs of active noise cancellation algorithms were obtained, as shown in Figure 4.5. Figure 4.6 shows a closer look at the last IN. The average value and the standard deviation of the power of output signals *e(n)* were calculated and utilized for evaluation (Table 4.1). Figure 4.7 shows a closer look at the last BS to observe corruptions caused by adapting algorithms. Correlation between output signal *e(n)* and bowel sound signal *s(n)* were calculated for evaluate corruptions. LMS and AL filter algorithm attenuates ambient noise effects the most while keeping bowel signals uncorrupted among other algorithms.

Table 4.3. Performance assessments of adaptive filter algorithms for simulation 3

Adapting Algorithm	**Computation Time (s)** $\boldsymbol{t}$		**Power of Error Signal (dB)** $\boldsymbol{P_{e(n)}}$		**Correlation** $\boldsymbol{Corr(e(n), s(n))}$	
	$\boldsymbol{\mu}$	$\boldsymbol{\sigma}$	$\boldsymbol{\mu}$	$\boldsymbol{\sigma}$	$\boldsymbol{\mu}$	$\boldsymbol{\sigma}$
LMS	0.0272	0.0014	0.9603	0.0908	0.9620	0.0038
NLMS	0.0333	0.0017	4.4116	0.2302	0.6464	0.0172
AP	5.7599	0.1087	4.4308	0.2469	0.6441	0.0171
RLS	13.1852	0.4335	1.1337	0.1146	0.9432	0.0102
AL	2.3666	0.0484	0.9445	0.0909	0.9639	0.0033

In simulation 4, multiple INs and BSs without BN were generated, and outputs of active noise cancellation algorithms were obtained, as shown in Figure 4.8. Figure 4.9 shows a closer look at the last IN. The average value and the standard deviation of the power of output signals *e(n)* were calculated and utilized for evaluation (Table 4.1). Figure 4.10 shows a closer look at the last BS to observe corruptions caused by adapting algorithms. Correlation between output signal *e(n)* and bowel sound signal *s(n)* was calculated to evaluate corruptions. AL filter algorithm attenuates ambient noise effects the most while keeping bowel signals uncorrupted, among other algorithms.

Table 4.4. Performance assessments of adaptive filter algorithms for simulation 4

Adapting Algorithm	**Computation Time (s)** $\boldsymbol{t}$		**Power of Error Signal (dB)** $\boldsymbol{P_{e(n)}}$		**Correlation** $\boldsymbol{Corr(e(n), s(n))}$	
	$\boldsymbol{\mu}$	$\boldsymbol{\sigma}$	$\boldsymbol{\mu}$	$\boldsymbol{\sigma}$	$\boldsymbol{\mu}$	$\boldsymbol{\sigma}$
LMS	0.0254	0.0016	-0.5568	0.1334	0.9763	0.0046
NLMS	0.0326	0.0012	-0.2078	1.0882	0.9441	0.0728
AP	5.4839	0.1508	-0.2032	0.4351	0.9393	0.0381
RLS	13.3520	0.2913	0.6395	5.0381	0.9288	0.2169
AL	2.3464	0.0402	-0.1796	2.0064	0.9522	0.1361

4.1.2. Results of ANC on real auscultation data

Selected adaptive filters were tested with ten different real auscultation recordings. An example of the input signal *x(n)*, the desired signal *d(n)* and output signals *e(n)* of the ANC application is shown in Figure 4.11. Figure 4.12 shows a closer look at an IN in this ANC application. The average value and the standard deviation of the power of output signals *e(n)* were calculated and utilized for evaluation (Table 4.5). Figure 4.13 shows a closer look at a BS to observe corruptions caused by adapting algorithms. Correlation between output signal *e(n)* and desired signal *d(n)* was calculated to evaluate corruptions. AL filter algorithm attenuates ambient noise effects the most while keeping bowel signals uncorrupted, among other adaptive filter algorithms.

Table 4.5. Performance assessments of adaptive filters on real auscultation data

Adapting Algorithm	Computation Time (s) t		Power of Error Signal (dB) $P_{e(n)}$		Correlation $Corr(e(n), d(n))$	
	μ	σ	μ	σ	μ	σ
LMS	0.0333	0.0198	1.7976	0.6153	0.6107	0.0229
NLMS	0.0355	0.0054	1.9433	0.7240	0.2211	0.0244
AP	5.8242	0.2407	1.8834	0.6396	0.2799	0.0087
RLS	13.5643	0.1616	1.8555	0.5568	0.6044	0.0315
AL	2.3652	0.0440	1.6847	0.6168	0.6159	0.0226

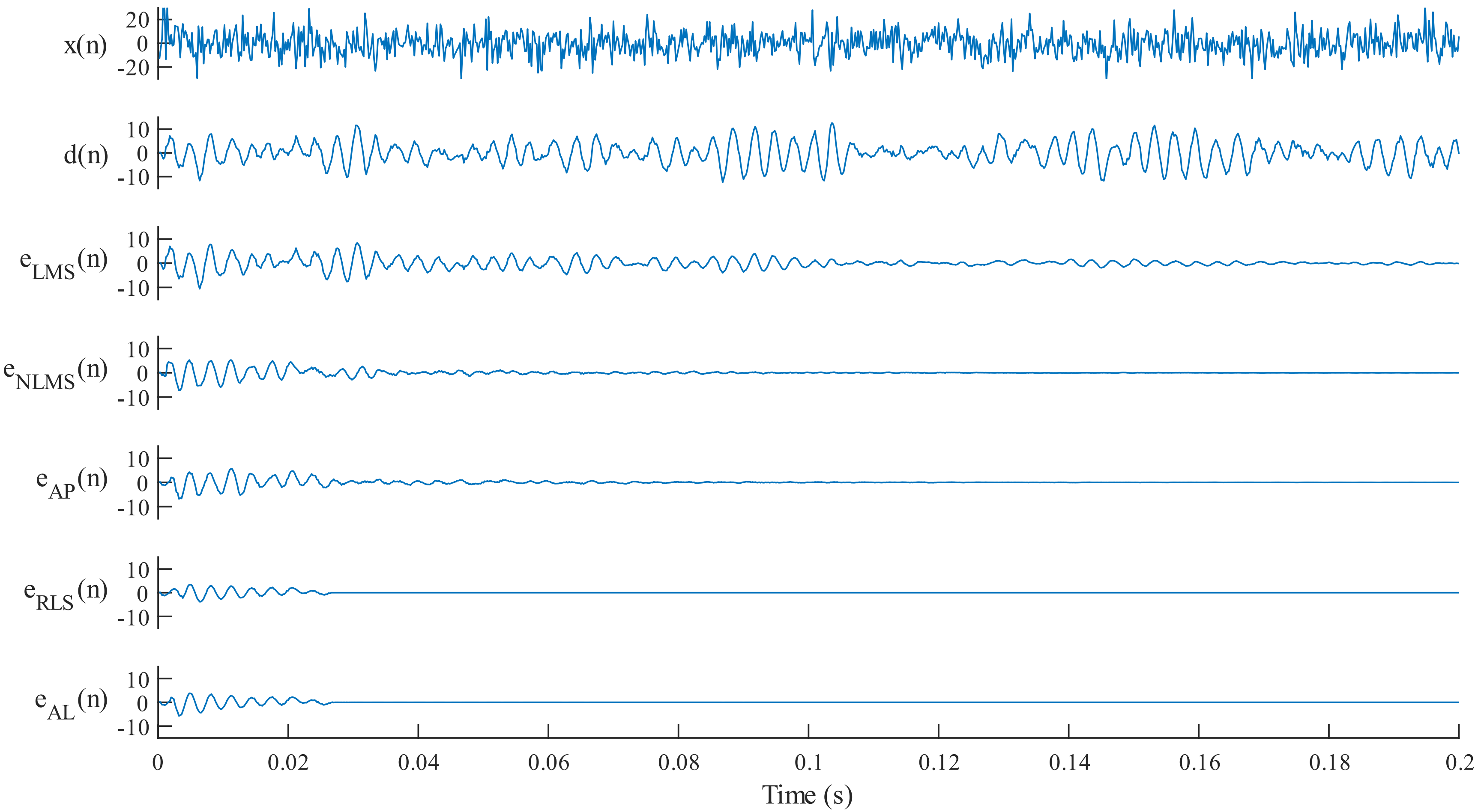

Figure 4.2. ANC application on synthetic data (simulation 1): an example of input signal and ANC outputs

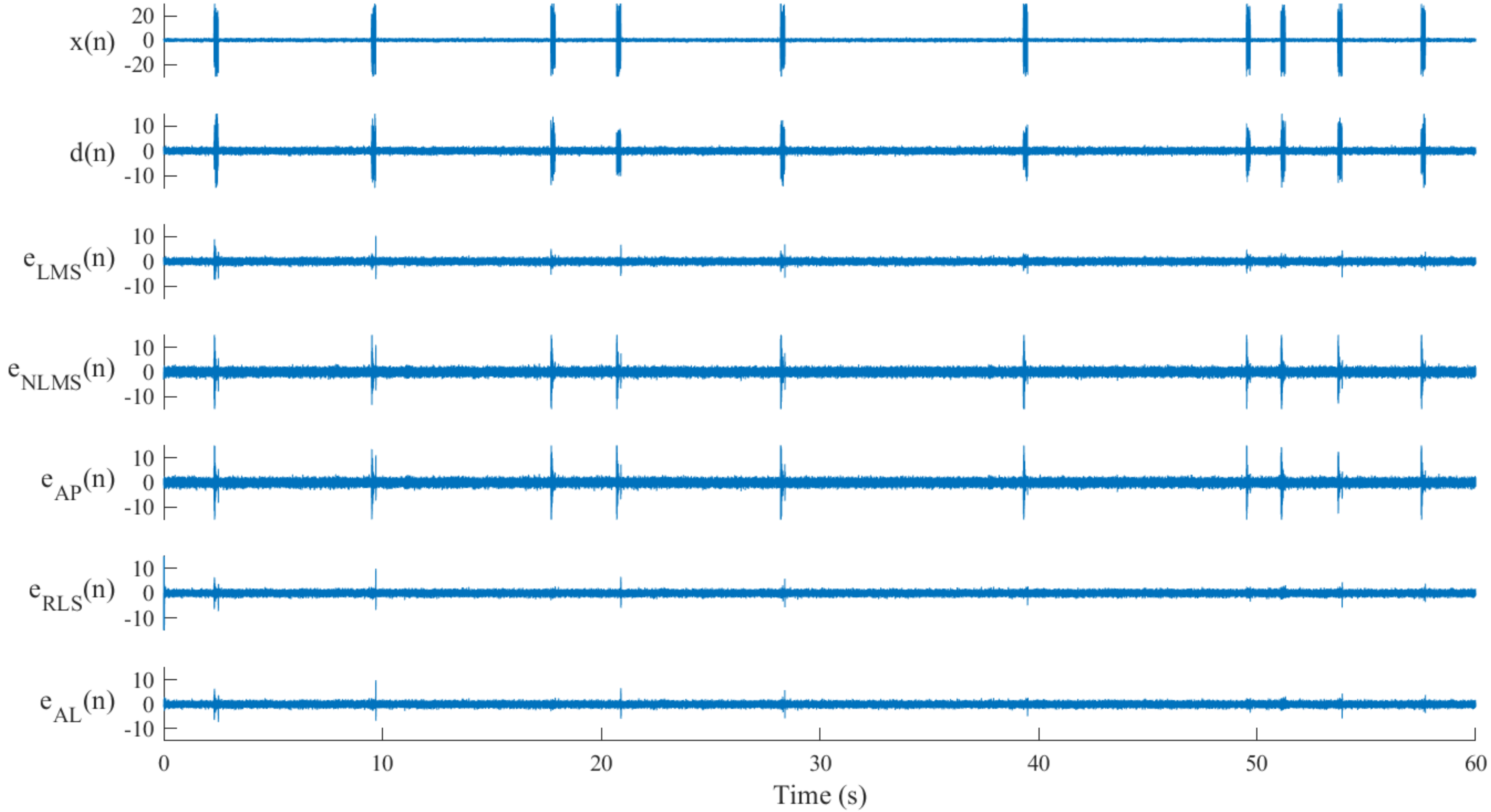

Figure 4.3. ANC application on synthetic data (simulation 2): an example of input signal and ANC outputs

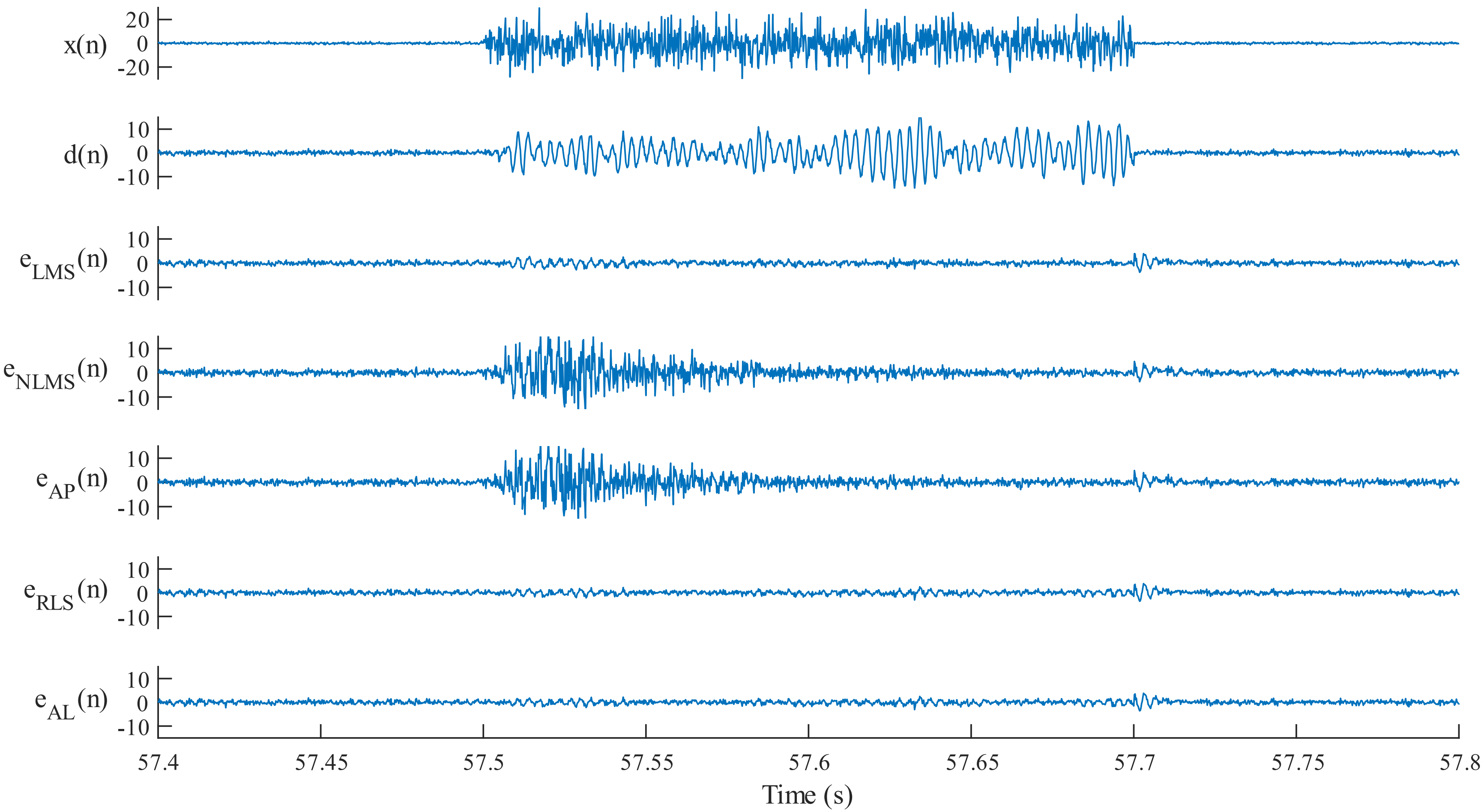

Figure 4.4. ANC application on synthetic data (simulation 2): an example of input signal and ANC outputs (a closer look at an IN)

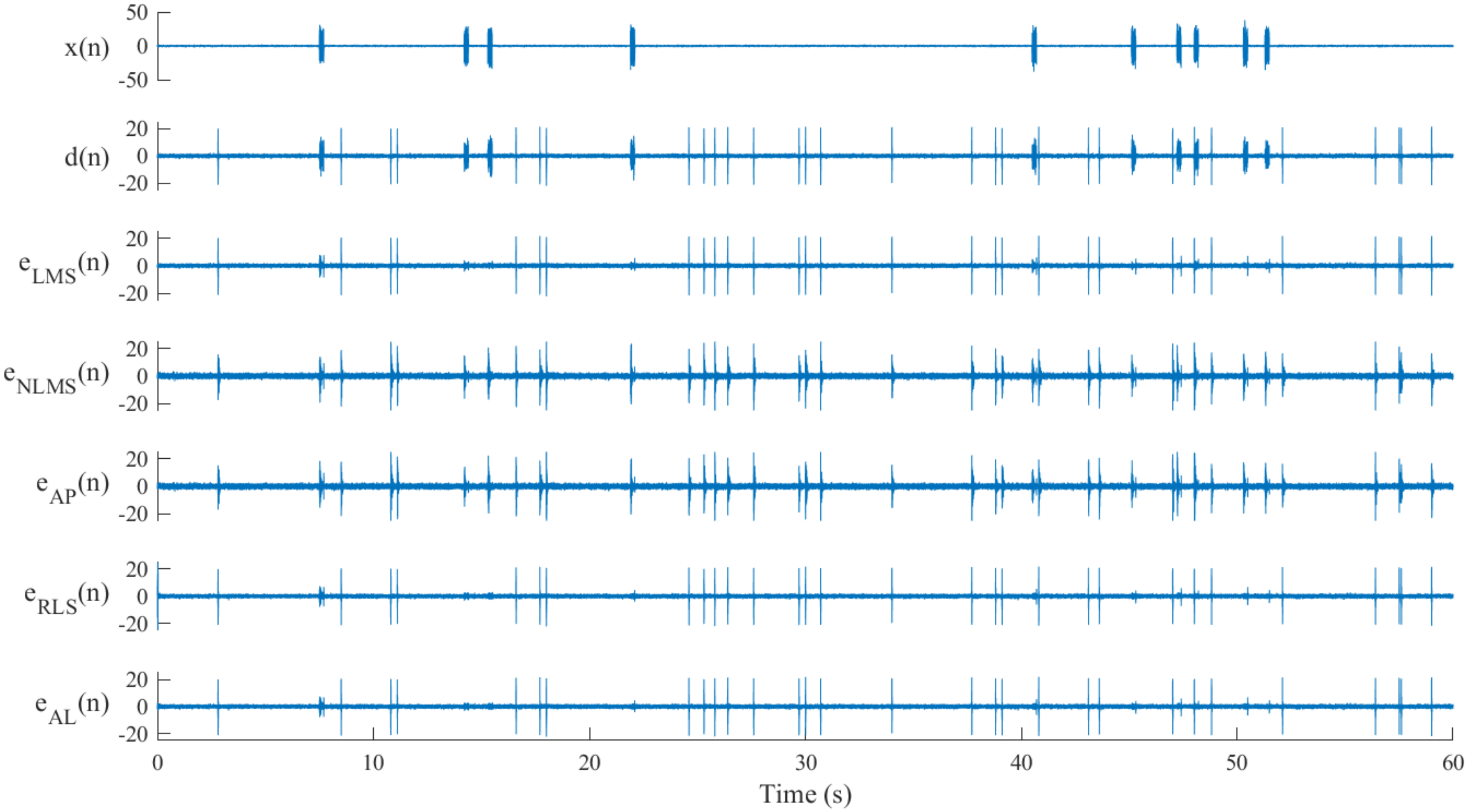

Figure 4.5. ANC application on synthetic data (simulation 3): an example of input signal and ANC outputs

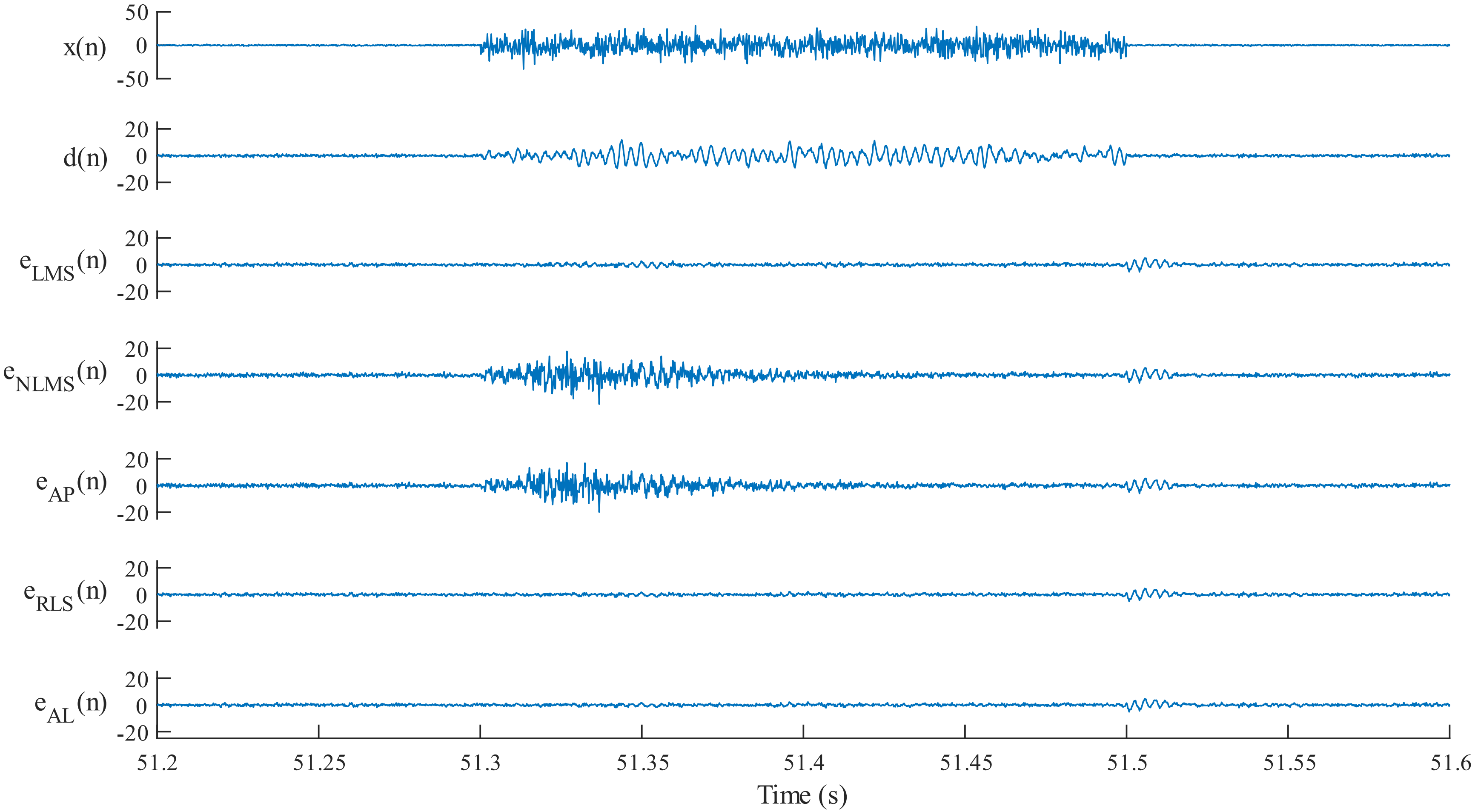

Figure 4.6. ANC application on synthetic data (simulation 3): an example of input signal and ANC outputs (a closer look at an IN)

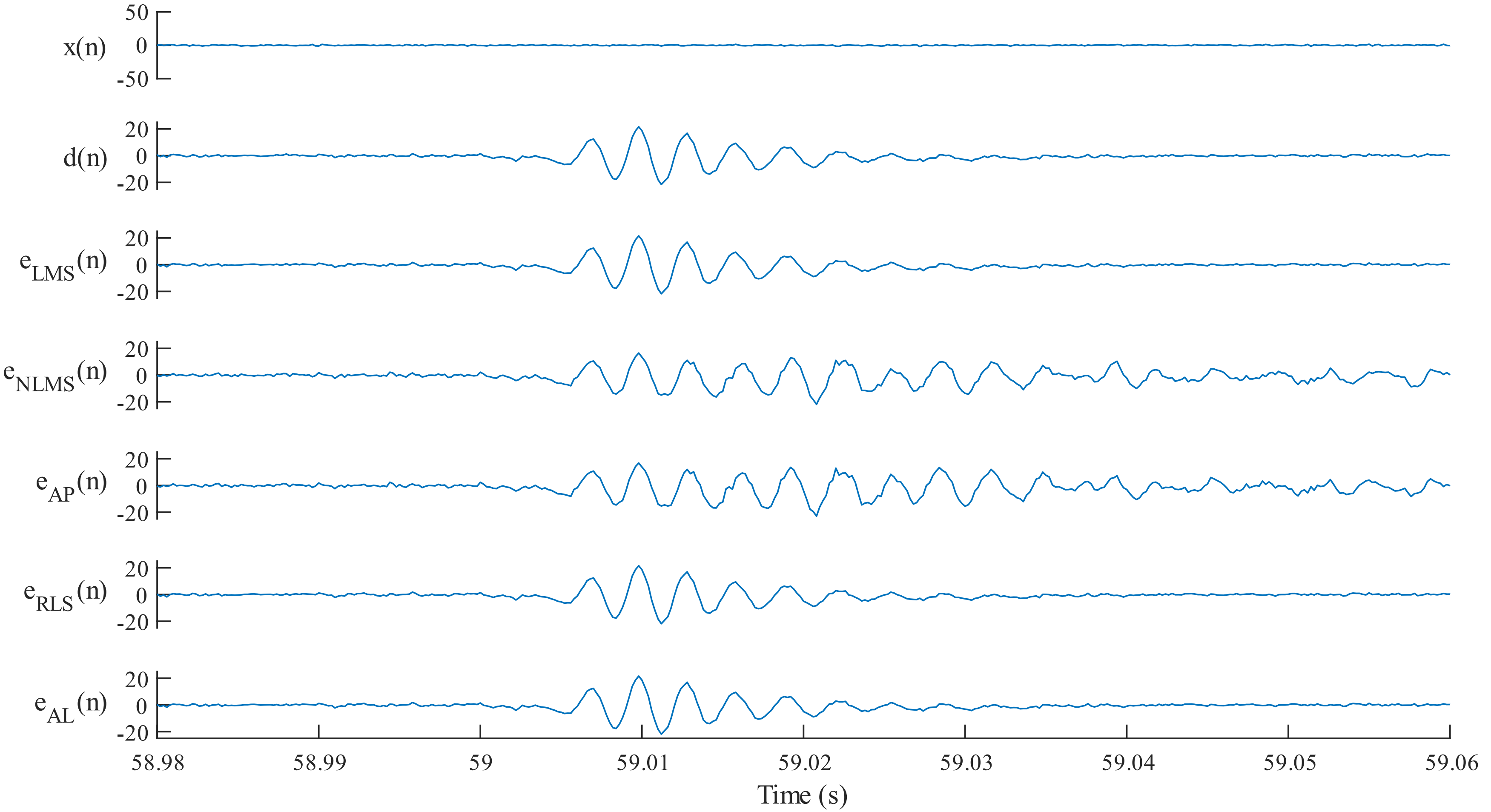

Figure 4.7. ANC application on synthetic data (simulation 3): an example of input signal and ANC outputs (a closer look at a BS)

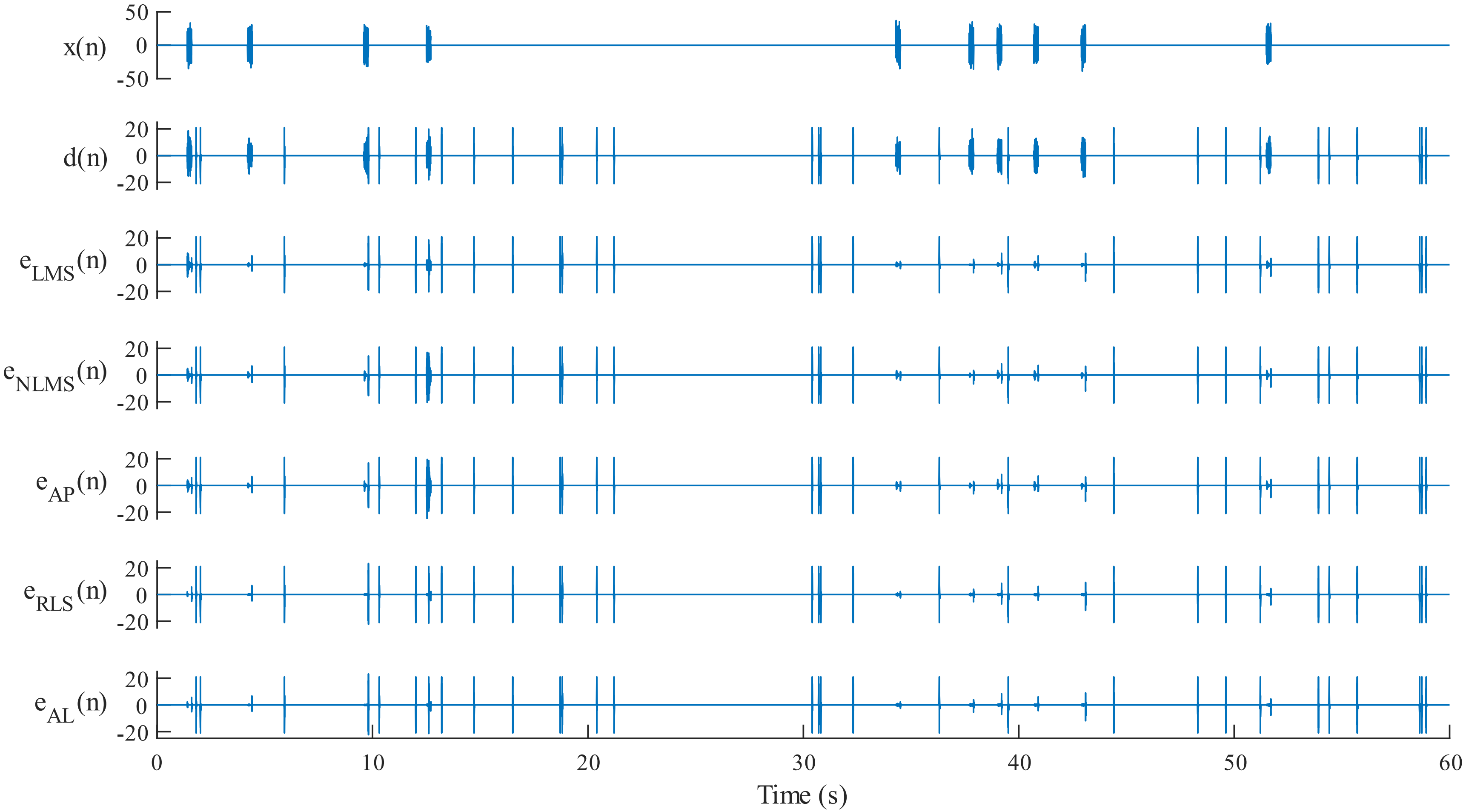

Figure 4.8. ANC application on synthetic data (simulation 4): an example of input signal and ANC outputs

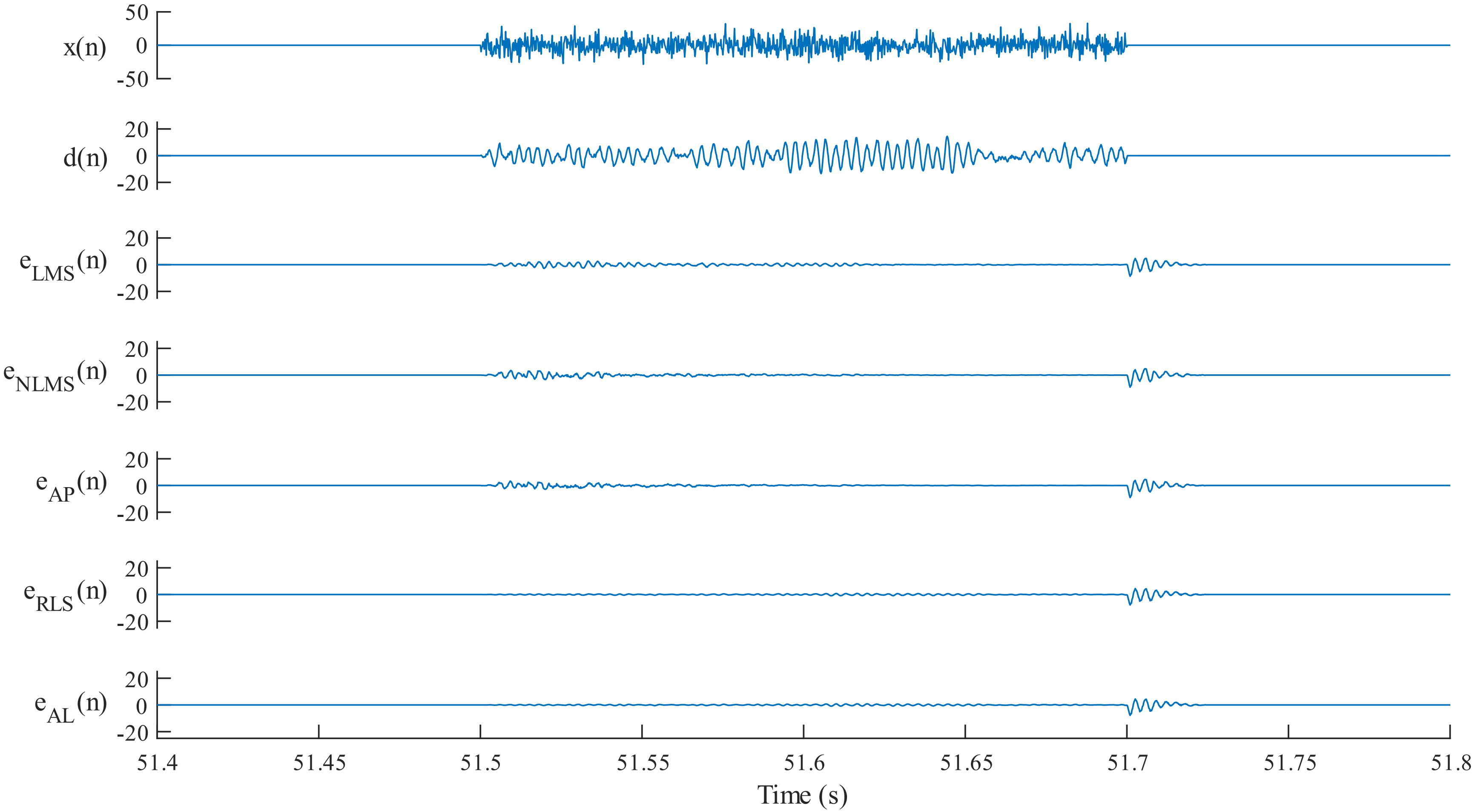

Figure 4.9. ANC application on synthetic data (simulation 4): an example of input signal and ANC outputs (a closer look at an IN)

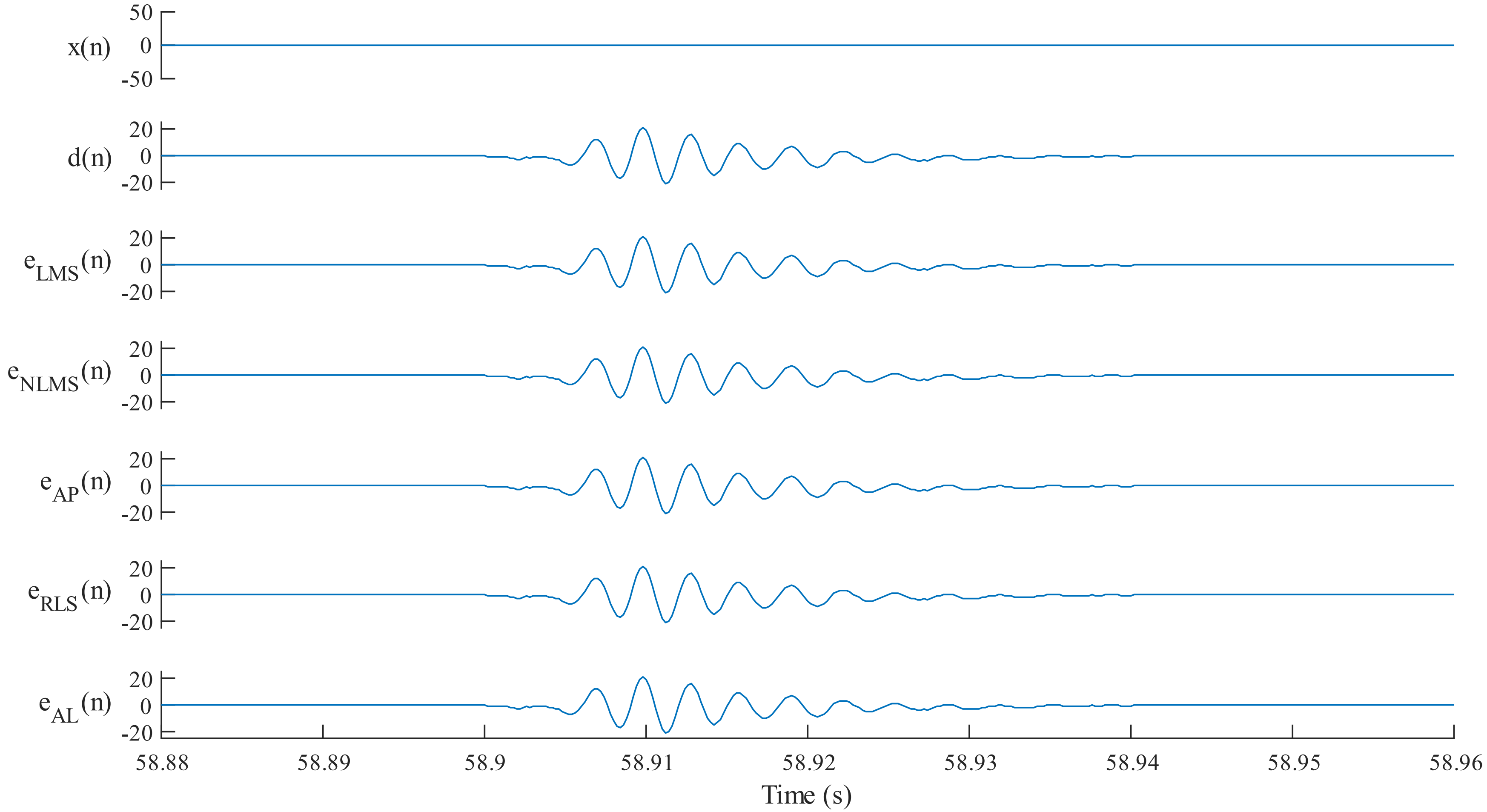

Figure 4.10. ANC application on synthetic data (simulation 4): an example of input signal and ANC outputs (a closer look at a BS)

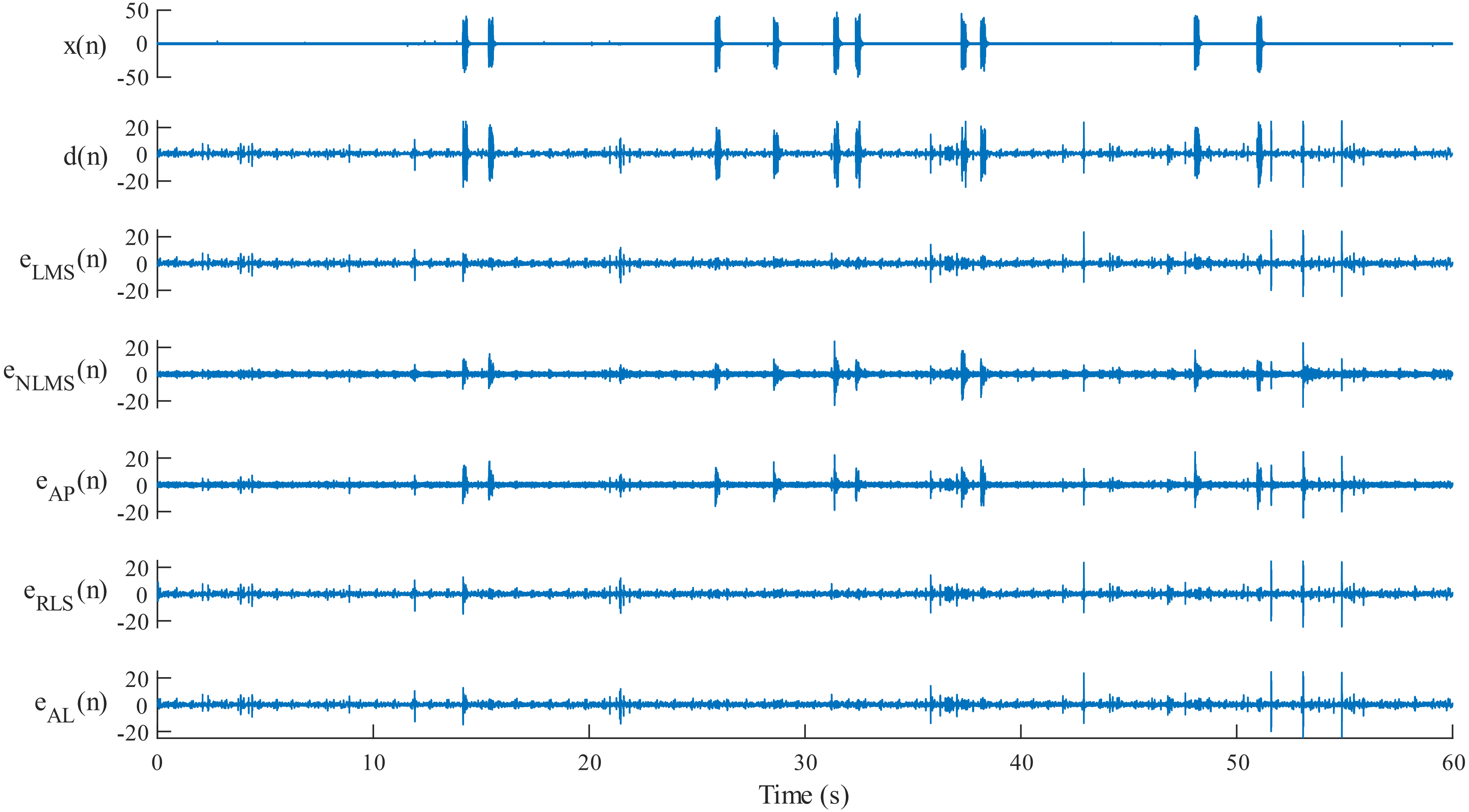

Figure 4.11. ANC application on real auscultation data: an example of input signal and ANC outputs

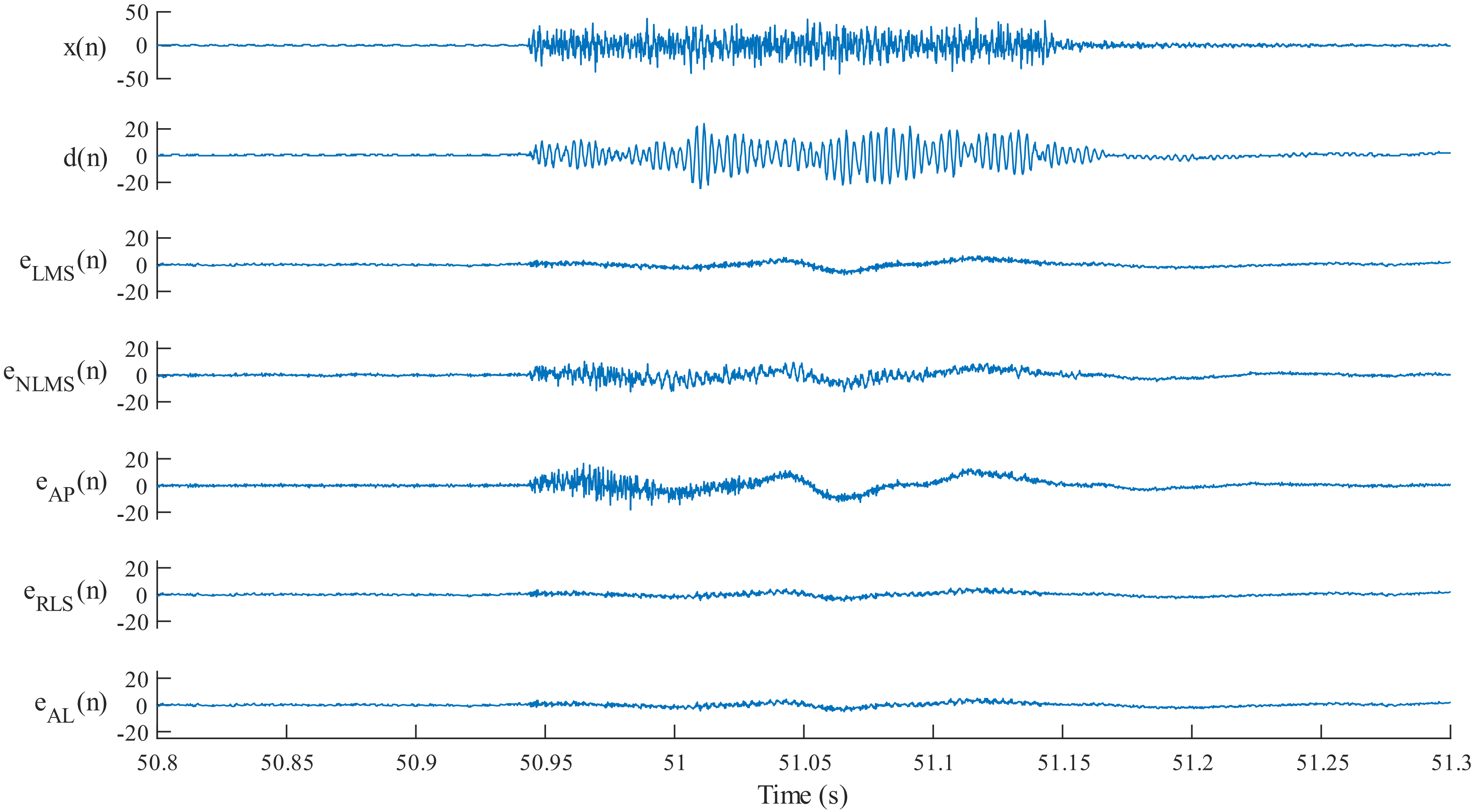

Figure 4.12. ANC application on real auscultation data: an example of input signal and ANC outputs (a closer look at an IN)

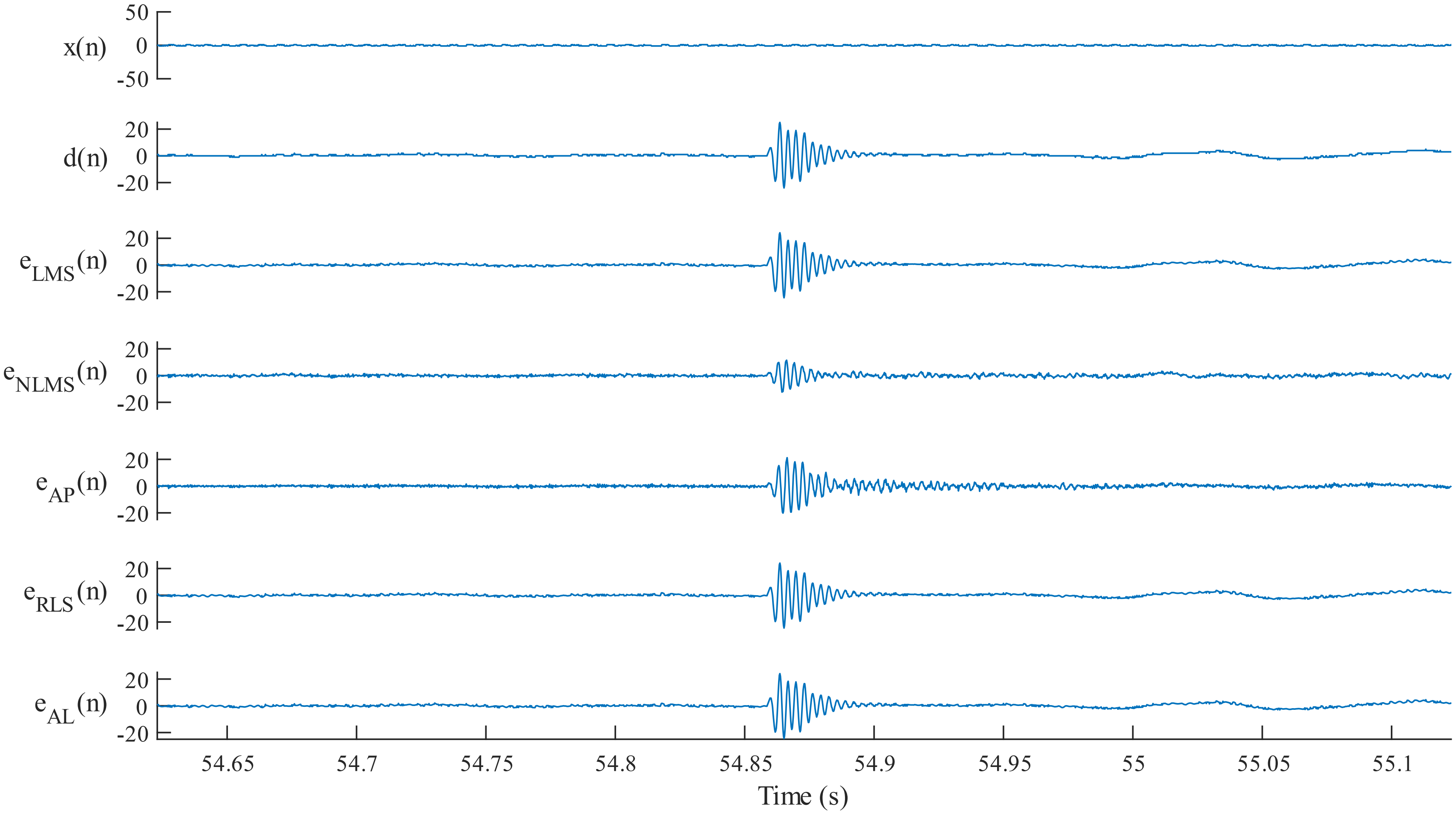

Figure 4.13. ANC application on real auscultation data: an example of input signal and ANC outputs (a closer look at a BS)

4.2. Results of Bowel Activity Detection

Bowel activity detection algorithm was tested with 10 different 60 seconds long real auscultation recordings. These recordings were collected with the test setup setting by generating random impulsive noises (10 IN per minute). Bowel activity regions in the signals were labelled by an expert. ROC curves were generated for each signal and the optimum threshold value identified from the ROC curves. Table 4.6 shows determined optimum thresholds values for each signal and corresponding performances obtained with these threshold values. The average threshold value was 3.07 times of the standard deviation of the auscultation signal. Average sensitivity, also known as true positive rate, was 0.9509. Average specificity, calculated as subtracting false positive rate from 1, was 0.9583.

Table 4.6. Bowel activity detection performances for each auscultation

Signal Number	Optimum Threshold	Sensitivity (TPR)	Specificity (1-FPR)
1	2.8900	0.8676	0.9114
2	3.5700	0.9607	0.9888
3	2.6900	1.0000	0.9343
4	2.9400	0.9575	0.9687
5	3.7518	0.9166	0.9650
6	2.5762	0.9714	0.9474
7	3.1752	0.9428	0.9614
8	2.8859	0.9354	0.9589
9	3.2776	0.9762	0.9863
10	2.9751	0.9807	0.9606
Average	**3.0732**	**0.9509±0.0379**	**0.9583±0.0230**

By using bowel activity detection algorithm, a few detection examples are shown below. Figure 4.14 shows an example of detected bowel activity while ambient noise is absent. Figure 4.15 shows an example of detected bowel activity while ambient noise exists. It can be clearly seen that, ambient noise observed with both microphones is filtered effectively and do not causes false positive detection. When bowel sound and ambient noise occur at the same time interval, ANC shows an effective noise reduction performance and BS signal is not affected from filtering process. An example case is shown in Figure 4.15.

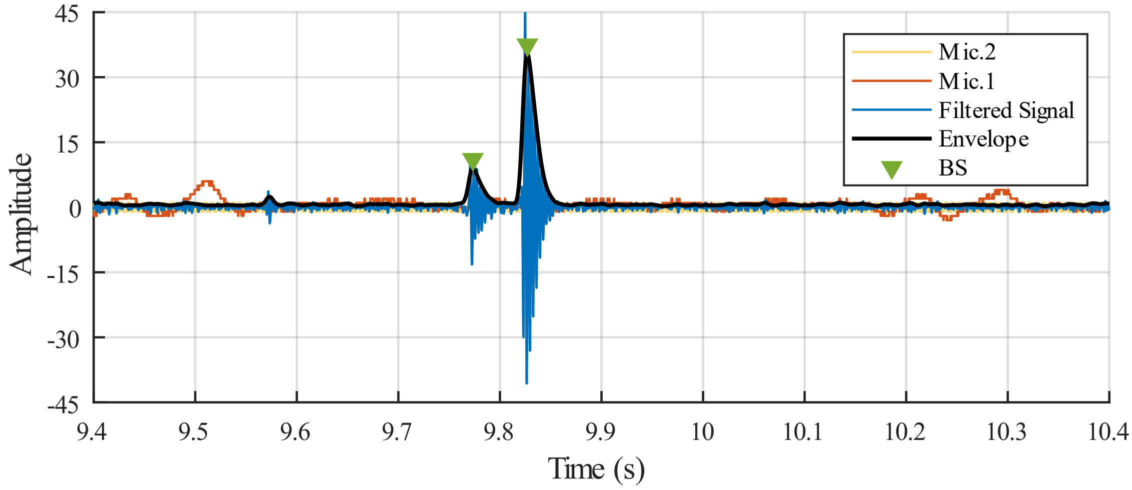

Figure 4.14. An example of detected bowel activity while noise is absent

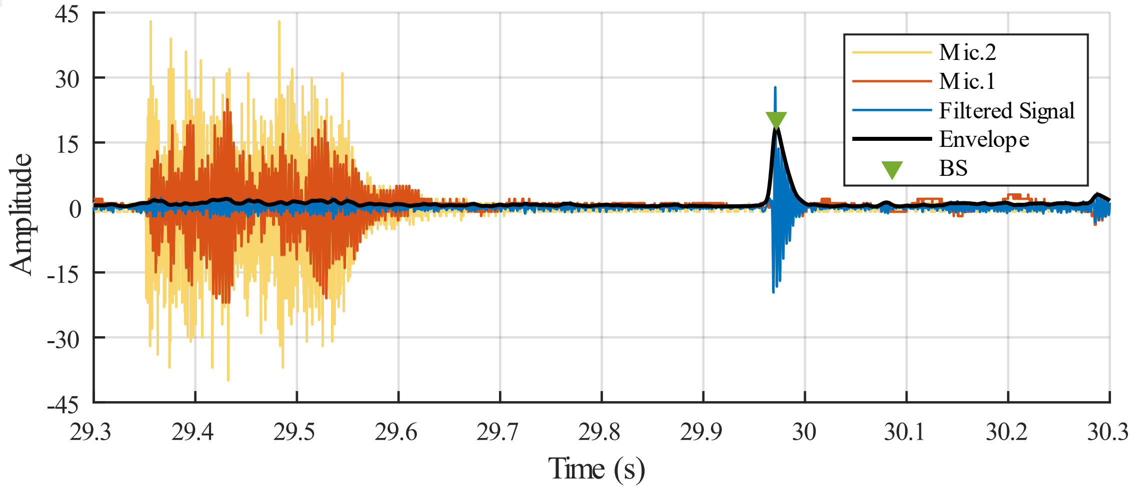

Figure 4.15. An example of detected bowel activity while noise exists

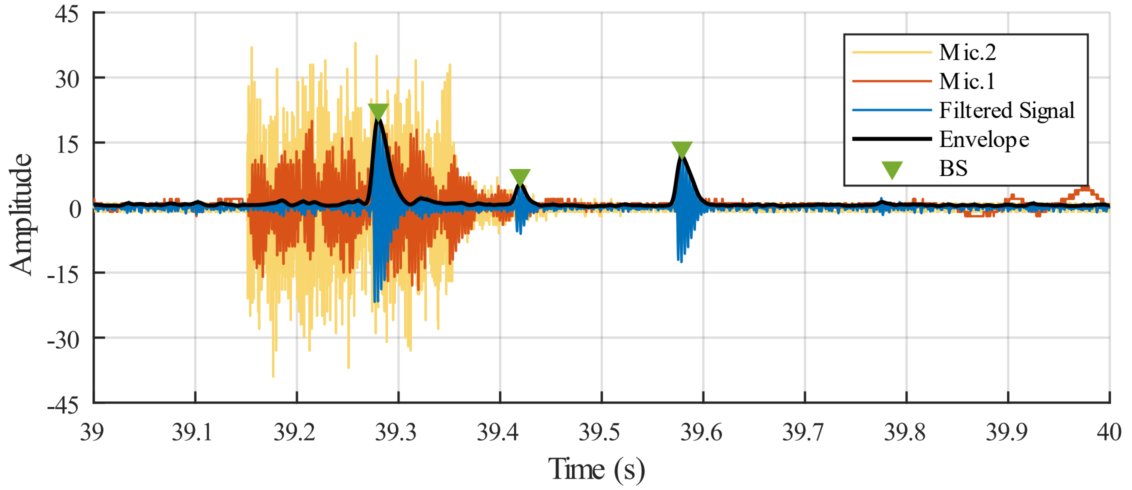

Figure 4.16. An example of detected bowel activity that coincides with the noise

5. CONCLUSION

Continuous monitoring of bowel activity is desirable to perform research on healing enhancement after surgery. Noise in clinical environments creates additional challenge for automated bowel sound detection systems. In this study, we have developed an effective active noise cancellation application by utilizing two microphones of the electronic stethoscope to increase detection accuracy. For the purpose of noise attenuation and bowel activity identification, a comprehensive review of active noise cancellation techniques and adaptive filters were performed, and various algorithms are tested. Finally, a bowel activity detection and noise attenuation algorithm were developed for our custom design IoT-driven electronic stethoscope.

Five different adaptive filter algorithms were tested for active noise cancellation. The adaptive lattice filter algorithm was selected for active noise cancellation due to its high noise reduction performance and acceptable computational cost. Adaptive filter performances were tested only with white Gaussian noises since it is the best and average model to represent any noise that occurs in nature. But this assumption may not be entirely valid for real clinical conditions. Adaptive filters may show slightly different performance on the real ambient noises observed in clinical conditions. Therefore, we aim to test and improve the active noise cancellation application with real auscultation data collected in a clinical environment.

The bowel activity detection algorithm was tested with ten different one-minute long auscultation recordings that are collected in a controlled environment. An expert has labeled the bowel activity regions in the auscultation recordings. A sensitivity of 95.09 ± 3.79% and a specificity of 95.83 ± 2,3% were obtained in bowel sound recognition. To detect bowel activity, Ulusar used a Naive Bayesian algorithm for bowel sound detection, and minimum statistics and spectral subtraction for noise reduction, achieving an overall recognition performance of 94.15% (Ulusar 2014). Kim et al. devised a modified iterative kurtosis-based detector algorithm for enhancing the denoising performance, and an estimation algorithm of bowel motility based on the regression modeling of the jitter and shimmer of BS signals (Kim et al. 2011). They achieved 86.3 ± 6.0% sensitivity and 91.0 ± 6.1% specificity in bowel sound detection. Yin et al. developed a bowel sound recognition algorithm using Support Vector Machine classification for a wearable health monitoring system and achieved 90% recognition performance (Yin et al. 2018). Dimoulas et al. used feedforward multilayer neural networks and observed 94.84% bowel activity recognition accuracy (Dimoulas et al. 2008).

The bowel activity detection algorithm was tested with only recorded auscultation data. For future studies, we are planning to improve bowel sound detection accuracy by using probabilistic and machine learning methods, and temporal, spectral, and statistical features of the bowel sound signals. Additionally, the algorithm will be implemented on our IoT-driven electronic stethoscope to detect bowel activity simultaneously. Although, the results of this study are quite promising, in order to assess the clinical usefulness of the system, auscultation records will be collected from a large diversity of patient population.

6. REFERENCES

Al-Sarawi, S., Anbar, M., Alieyan, K., and Alzubaidi, M. 2017. Internet of Things (IoT) communication protocols: Review. 2017 8th International Conference on Information Technology (ICIT), pp. 685–690.

Al-Turjman, F., Nawaz, M.H., and Ulusar, U.D. 2020. Intelligence in the Internet of Medical Things era: A systematic review of current and future trends. *Comput. Commun.*, 150: 644–660.

Dimoulas, C., Kalliris, G., Papanikolaou, G., and Kalampakas, A. 2006. Novel wavelet domain Wiener filtering de-noising techniques: Application to bowel sounds captured by means of abdominal surface vibrations. *Biomed. Signal Process. Control*, 1: 177–218.

Dimoulas, C., Kalliris, G., Papanikolaou, G., and Kalampakas, A. 2007. Long-term signal detection, segmentation and summarization using wavelets and fractal dimension: A bioacoustics application in gastrointestinal-motility monitoring. *Comput. Biol. Med.*, 37: 438–462.

Dimoulas, C., Kalliris, G., Papanikolaou, G., Petridis, V., and Kalampakas, A. 2008. Bowel-sound pattern analysis using wavelets and neural networks with application to long-term, unsupervised, gastrointestinal motility monitoring. *Expert Syst. Appl.*, 34: 26–41.

Diniz, P.S.R. 2020. Adaptive Filtering: Algorithms and Practical Implementation. Springer International Publishing, 495 p.

Emoto, T., Shono, K., Abeyratne, U.R., Okahisa, T., Yano, H., Akutagawa, M., Konaka, S., and Kinouchi, Y. 2013. ARMA-based spectral bandwidth for evaluation of bowel motility by the analysis of bowel sounds. *Physiol. Meas.*, 34: 925–936.

Frank, P.-W.L., and Meng, M.Q.-H. 2016. A low cost Bluetooth powered wearable digital stethoscope for cardiac murmur. 2016 IEEE International Conference on Information and Automation (ICIA), pp. 1179–1182.

Hadjileontiadis, L.J. 2005a. Wavelet-based enhancement of lung and bowel sounds using fractal dimension thresholding-part I: methodology. *IEEE Trans. Biomed. Eng.*, 52: 1143–1148.

Hadjileontiadis, L.J. 2005b. Wavelet-based enhancement of lung and bowel sounds using fractal dimension thresholding-part II: application results. *IEEE Trans. Biomed. Eng.*, 52: 1050–1064.

Hadjileontiadis, L.J., and Rekanos, I.T. 2003. Detection of explosive lung and bowel sounds by means of fractal dimension. *IEEE Signal Process. Lett.*, 10: 311–314.

Hamlet, S., Penney, D.G., and Formolo, J. 1994. Stethoscope acoustics and cervical auscultation of swallowing. *Dysphagia*, 9: 63–68.

Haykin, S. 2013. Adaptive Filter Theory. Pearson, 912 p.

Jatupaiboon, N., Pan-ngum, S., and Israsena, P. 2010. Electronic stethoscope prototype with adaptive noise cancellation. 2010 Eighth International Conference on ICT and Knowledge Engineering, pp. 32–36.

Jiao, Y., Cheung, R.Y.P., Chow, W.W.Y., and Mok, M.P.C. 2013. A novel gradient adaptive step size LMS algorithm with dual adaptive filters. 2013 35th Annual International Conference of the IEEE Engineering in Medicine and Biology Society (EMBC), pp. 4803–4806.

Kim, K.S., Seo, J.H., Ryu, S.H., Kim, M.H., and Song, C.G. 2011. Estimation algorithm of the bowel motility based on regression analysis of the jitter and shimmer of bowel sounds. *Comput. Methods Programs Biomed.*, 104: 426–434.

Ou, D., OuYang, L., Tan, Z., Mo, H., Tian, X., and Xu, X. 2016. An electronic stethoscope for heart diseases based on micro-electro-mechanical-system microphone. 2016 IEEE 14th International Conference on Industrial Informatics (INDIN), pp. 882–885.

Rizk, M., and Wolf, P.D. 2009. Optimizing the automatic selection of spike detection thresholds using a multiple of the noise level. *Med. Biol. Eng. Comput.*, 47: 955–966.

Schroeder, D., Gillanders, L., Mahr, K., and Hill, G.L. 1991. Effects of Immediate Postoperative Enteral Nutrition on Body Composition, Muscle Function, and Wound Healing. *J. Parenter. Enter. Nutr.*, 15: 376–383.

Tang, Y., Cao, G., Li, H., and Zhu, K. 2010. The Design of Electronic Heart Sound Stethoscope Based on Bluetooth. 2010 4th International Conference on Bioinformatics and Biomedical Engineering, pp. 1–4.

Türk, E., Öztaş, A.S., Deniz Uluşar, Ü., Canpolat, M., Kazanır, S., Yaprak, M., Öğünç, G., Doğru, V., and Canagir, O.C. 2015. Wireless bioacoustic sensor system for automatic detection of bowel sounds. 2015 19th National Biomedical Engineering Meeting (BIYOMUT), pp. 1–4.

Ulusar, U.D. 2014. Recovery of gastrointestinal tract motility detection using Naive Bayesian and minimum statistics. *Comput. Biol. Med.*, 51: 223–228.

Ulusar, U.D., Canpolat, M., Yaprak, M., Kazanir, S., and Ogunc, G. 2013. Real-time monitoring for recovery of gastrointestinal tract motility detection after abdominal surgery. 2013 7th International Conference on Application of Information and Communication Technologies, pp. 1–4.

Ulusar, U.D., Al-Turjman, F., and Celik, G. 2017. An overview of Internet of things and wireless communications. 2017 International Conference on Computer Science and Engineering (UBMK), pp. 506–509.

Ulusar, U.D., Turk, E., Oztas, A.S., Savli, A.E., Ogunc, G., and Canpolat, M. 2019. IoT and Edge Computing as a Tool for Bowel Activity Monitoring. Edge Computing: From Hype to Reality, F. Al-Turjman, ed. (Cham: Springer International Publishing), pp. 133–144.

Vaseghi, S.V. 2008. Advanced Digital Signal Processing and Noise Reduction. John Wiley & Sons, 547 p.

Yin, Y., Jiang, H., Feng, S., Liu, J., Chen, P., Zhu, B., and Wang, Z. 2018. Bowel sound recognition using SVM classification in a wearable health monitoring system. *Sci. China Inf. Sci.*, 61: 084301.

RESUME

Erdinç TÜRK

erdincturk@akdeniz.edu.tr

EDUCATION

Master of Science 2017-2020	Akdeniz University Institute of Natural and Applied Sciences, Computer Engineering, Antalya, Turkey
Bachelor of Science 2008-2014	Akdeniz University Faculty of Engineering, Electrical Electronics Engineering, Antalya, Turkey

WORK EXPERIENCE

Research Assistant 04/2017-Present	Akdeniz University Faculty of Engineering, Computer Engineering, Antalya, Turkey

PUBLICATIONS

1- Türk, E., Öztaş, A.S., Deniz Uluşar, Ü., Canpolat, M., Kazanır, S., Yaprak, M., Öğünç, G., Doğru, V., and Canagir, O.C. 2015. Wireless bioacoustic sensor system for automatic detection of bowel sounds. In 2015 19th National Biomedical Engineering Meeting (BIYOMUT), pp. 1–4.

2- Ulusar, U.D., Celik, G., Turk, E., Al-Turjman, F., and Guvenc, H. 2018. Accurate Indoor Localization for ZigBee Networks. In 2018 3rd International Conference on Computer Science and Engineering (UBMK), pp. 514–517.

3- Ulusar, U.D., Turk, E., Oztas, A.S., Savli, A.E., Ogunc, G., and Canpolat, M. 2019. IoT and Edge Computing as a Tool for Bowel Activity Monitoring. In Edge Computing: From Hype to Reality, F. Al-Turjman, ed. (Cham: Springer International Publishing), pp. 133–144.

4- Ulusar, U.D., Celik, G., Turk, E., Al-Turjman, F., and Guvenc, H. 2019. Practical Performability Assessment for ZigBee-Based Sensors in the IoT Era. In Performability in Internet of Things, F. Al-Turjman, ed. (Cham: Springer International Publishing), pp. 21–31.